Title

Physicocochemical Properties of Escanaba Trough Sediments

Author

Tidwell, Jacob

Publication Date

2024

UNIVERSITY OF CALIFORNIA

SANTA CRUZ

PHYSICOCHEMICAL PROPERTIES OF ESCANABA TROUGH SEDIMENTS

A thesis submitted in partial satisfaction of

the requirements for the degree of

MASTER OF SCIENCE

in

EARTH SCIENCES

by

Jacob Tidwell

March 2024

The Thesis of Jacob Tidwell

is approved:

Professor Andrew Fisher

Dr. Amy Gartman

Professor Elise Knittle

Peter Biehl

Vice Provost and Dean of Graduate Studies

Table of Contents

List of Figures and Tables

Figures

Tables

Abstract

Physicochemical Properties of Escanaba Trough Sediments

by

Jacob Tidwell

Escanaba Trough, located on the Southern segment of the Gorda Ridge, is a mid-ocean spreading center filled with turbidites from the West Coast of North America. The high contrast in density between the sediment that fills the trough and the minerals that precipitate from hydrothermal fluid provide ideal conditions for using physical methods to determine the lateral extent of hydrothermal mineralization on the seafloor. This study reports results from sediment and rock sampling and analysis to evaluate the nature and spatial (surface) extent of hydrothermal influence in recovered materials. X-ray computed tomography (CT) scanning of push cores taken at intervals moving from the edge of vent sites to the distal seafloor shows that sediments primarily composed of hydrothermal minerals are constrained to within approximately 20 m of vent sites at seven of eight sites. However, positive europium anomalies are observed for every sediment sample taken at Escanaba Trough, suggesting hydrothermal influence is widespread throughout Escanaba Trough.

Acknowledgments

Thank you, first and foremost, to my advisor and mentor, Amy Gartman. Her guidance honed my scientific reasoning and reinforced my curiosity and passion for exploration. Amy is a brilliant scientist always willing to discuss new ideas. I would also like to thank Andrew Fisher and Elise Knittle. Andy offered me a home away from home in his lab and Elise was the perfect guide for learning how to be a TA. At USGS, SeanPaul La Selle provided a roadmap for working with data produced by the CT scanner at the Pacific Coastal and Marine Science Center that was invaluable.

Thank you to the Captain, officers and crew of the R/V Thomas G. Thompson, as well as the ROV Jason team for collecting the push cores and Pete Dal Ferro and Paul Knorr for their work collecting gravity cores. We thank Angela Tan for her work analyzing grain size, and Jay Padgett and Brooke Santos for their assistance with core logging. The project that inspired this thesis, Escanaba Trough: Exploring the Seafloor and Oceanic Footprints is an interagency effort involving the National Oceanic and Atmospheric Administration, the U.S. Geological Survey, and the Bureau of Ocean Energy Management. Funding is acknowledged from NOAA Ocean Exploration via its Ocean Exploration Fiscal Year 2019 Funding Opportunity and through the National Oceanographic Partnership Program (NOPP), from the USGS Coastal and Marine Hazards and Resources Enhanced Funding Opportunities, and from the Bureau of Ocean Energy Management through Interagency Agreement M19PG00021 with the United States Geological Survey.

1 Introduction

1.1 Hydrothermal vent sites and potential mineral resources

Seafloor hydrothermal vent sites form from water-rock and water-water interaction during the discharge of highly reacted fluid, following flow at elevated temperatures through rocks ± sediment, forming chimneys and mounds of primarily sulfide and sulfate minerals. Hydrothermal discharge sites can host unique biological communities, and associated mineral occurrences can contain high concentrations of industrially valuable elements such as Cu, Zn, Pb, Au, and Ag (Tivey, 2007). These mineral occurrences associated with hydrothermal vents sites are often referred to as seafloor massive sulfide "deposits." In the field of economic geology, any accumulation of minerals is called a "mineral occurrence." A mineral occurrence is termed a deposit when it is of large enough size and high enough grade for mining "under the most favorable of circumstances" (Cox and Singer, 1986). There is generally not sufficient information on seafloor mineral occurrences to determine whether or not they constitute deposits in this sense. There has been no commercial mining of seafloor massive sulfides as of 2024, although there is continued interest in understanding which hydrothermal systems may generate mineral deposits, evaluating the composition and extent of hydrothermal minerals in these locations, and understanding environmental impacts (Van Dover, 2010, Van Dover et al., 2020).

As a potential resource, seafloor massive sulfide occurrences offer a unique opportunity for intensive research prior to potential exploitation. Hydrothermal vent systems were only first observed in 1977 (Corliss et al., 1979), and much of the subsequent research has focused on locations where venting is active. There is comparatively less research on the footprint of hydrothermal vent sites on the seafloor, that is, a vent site's geochemical and physical influence on surrounding areas. Vent sites differ from the surrounding seafloor in several ways. The sulfide and sulfate minerals that accumulate around high-temperature vent sites, those with fluid temperatures > 200°C, are far more abundant in areas of the seabed with hydrothermal venting than those without. High-temperature vent fluids also have geochemical characteristics that differentiate them from seawater (Tivey, 2007).

1.2 Sedimented spreading centers

Vent sites at sediment-filled axial valleys of mid-ocean ridges differ from those in rock-dominated spreading centers in several ways. Sedimented spreading centers are typically found where new seafloor is created relatively close to continental margins, allowing larger rivers to deliver sediment rapidly to continental shelves and the deep ocean. Previous studies of sedimented vent sites like Middle Valley and Escanaba Trough have hypothesized that sulfide occurrences may be larger than those accumulating on bare-rock ridges (Fouquet et al., 1998). It has been asserted that among terrestrial massive sulfide deposits, those hosted in sedimentary rock are less abundant but larger (Goodfellow and Zierenberg, 1997). Sediment fill in spreading centers is less permeable than the upper basaltic volcanic basement, limiting advective heat extraction (Davis and Fisher, 1994). Some have argued this results in a more concentrated fluid flow, allowing for greater sulfide accumulation (Goodfellow and Zierenberg, 1997). Others have suggested fluids from vent sites at sediment filled spreading centers may deposit most of their metal below the seabed (Hannington et al., 2005). More recent analysis of terrestrial volcanogenic massive sulfide deposits, formed in environments akin to seafloor massive sulfides, indicates that those formed in siliciclastic-mafic environments like Escanaba Trough and Middle Valley aren't significantly larger than those formed in mafic bare rock settings (Mosier et al., 2009).

1.3 Rare earth element patterns of vent sites

The rare earth element (REE) profiles of hydrothermal fluids and minerals are one way they are differentiated from fluids and minerals formed from other processes. High-temperature vent fluids display similar REE characteristics at both sediment-hosted and volcanic rock vent sites: light rare earth element enrichment and a positive europium anomaly. Plagioclase phenocrysts present in rocks undergoing hydrothermal alteration have been identified as the primary source of REEs in hydrothermal fluids (Klinkhammer et al., 1994). Albitization is the alteration of the Ca end member of plagioclase, anorthite ($CaAl_2Si_2O_8$), to the Na end member, albite ($NaAlSi_3O_8$) (Bailey and Grabham, 1909). The replacement of Ca with Na causes a flux of Ca from the crust to the high-temperature fluid. Most REEs are in a trivalent state but Eu can be divalent at higher temperatures and pressures, like those in some vent fluid. Trivalent REE have a similar ionic radius to Ca, and can substitute for Ca in anorthite. When Ca is mobilized in vent fluid during albitization, the fluid is also enriched in REE, particularly Eu, relative to the other REEs (Olivarez and Owen, 1991). Deep sea sediments have been shown to scavenge REEs from the water column, and exhibit REE profiles which reflect the composition of the seawater and pore water to which they are exposed (Deng et al., 2017). Similarly, iron oxide and oxyhydroxide particulates in vent fluid scavenge REEs from vent fluid and the water column before being deposited on the seabed (German et al., 1990). This allows for the REE profile of vent fluid to be represented in deep-sea sediment.

However, similar REE patterns are also observed in ultra-mafic hosted vent sites where plagioclase is scarce. Either plagioclase-rich rocks are present but not observed, or other conditions like pH and redox play an important role in REE patterns (Douville et al., 2002). Experimental work has further indicated that elevated Cl and reduced fluid interacting with ultramafic rock can yield REE mobilization as well as the positive Eu anomaly, which is characteristic of hydrothermal fluids in the absence of plagioclase (Allen and Seyfried, 2005). Earlier studies of Eu anomalies in basalt have argued for the importance of redox conditions in addition to crystal chemistry (Towell et al., 1969).

1.4 Inactive vent sites

Given that high-temperature hydrothermal fluids are used to locate hydrothermal vents, one understudied class of vent sites is those that are no longer actively venting hydrothermal fluid. Vent sites without active venting are termed “inactive” or “extinct” (Jamieson and Gartman, 2020) and generally lack both readily detectable water-column thermal and chemical anomalies that can be mapped with ship-based surveys and seafloor biological communities that can be mapped efficiently with autonomous surveys. Inactive vent sites may preserve hydrothermal material and chemical signatures of high-temperature venting. Constraining the extent of hydrothermal material and chemical signatures on the seabed surrounding vent sites may help with the identification of extinct vent sites buried by sediment. Extinct vent sites buried by sediment are of interest because their burial may prevent the oxidative dissolution of sulfide minerals (Findlay et al., 2020).

1.5 Sampling vent sites

Taking samples from the regions beneath seafloor hydrothermal vent sites has historically required scientific drill ships like the JOIDES *Resolution* (Zierenberg et al., 1998). Recovered drill cores provide a window into the otherwise unseen subsurface of vent sites. The JOIDES *Resolution* is slated for retirement in 2024, with no planned replacement. In the absence of scientific drilling platforms, shallower core samples taken using widely available remotely operated vehicles (ROVs) can provide information on the understudied distal influence of vents sites on the surrounding seabed. Vent sites in regions with extensive sedimentation offer ideal conditions for distal sampling via ROV push coring. Push cores are relatively easy to collect in soft sediment, and allow for sampling informed by visible features, in contrast to gravity coring from the surface. However, sedimented spreading centers are relatively uncommon on a global basis, comprising perhaps 5% of active spreading centers (Hannington et al., 2005). Among these is Escanaba Trough.

1.6 Escanaba Trough

Escanaba Trough is the southernmost segment of the Gorda Ridge and the only active mid-ocean-ridge type spreading center in the exclusive economic zone of the United States (Figure 1A). Escanaba Trough is classified as a slow-spreading center opening at ~24 mm/year (full rate). The northern section of Escanaba is narrower than the southern section, 5 km wide vs 15 km wide (Fouquet et al., 1998). The Escanaba Trough is filled with sandy to silty turbidites and hemipelagic sediment between 300 m and 600 m thick, most of which was derived from the Columbia River and Klamath River Basins (Vallier et al., 1973; Zierenberg et al., 1994).

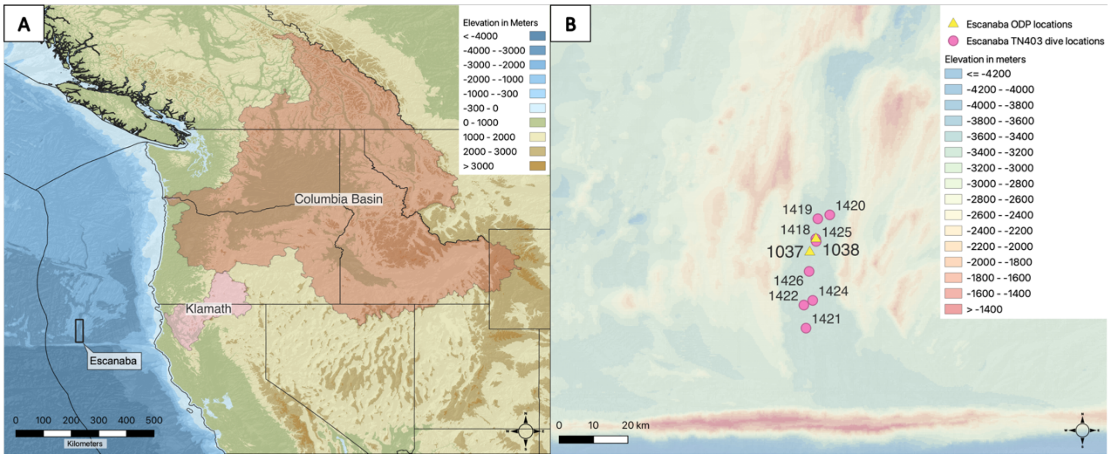

Figure 1. Regional and local maps showing study location. A. Regional map showing location of Escanaba Trough off the coast of Northern California. Major drainage basins delivering sediment to the continental margin are shown. B. Survey locations in southern Escanaba Trough labeled with ROV dive numbers. Ocean Drilling Project drill holes 1037 and 1038 are shown as yellow triangles. TN-403 ROV dives are shown as pink circles.

The provenance of the sediment in the Escanaba Trough is believed to be the Columbia River Basin and the rivers draining the Klamath Mountains based on the abundance of clinopyroxene and metamorphic amphibole minerals respectively (Normark et al., 1994). Sedimentation rates at Escanaba Trough have been linked with changes in sea level (Normark et al., 1994). Periods of lower sea level correspond to higher sedimentation rates, as major rivers flowed across the exposed continental shelf adjacent to North America and delivered sediment more rapidly into the deep ocean. One proposed model for sedimentation of Escanaba Trough suggests that the upper 150 m of sediment fill in the trough accumulated from 30 to 11 ka, corresponding to the Last Glacial Maximum and the associated (most recent) sea level low stand (Normark et al., 1994). Pleistocene sedimentation rates are estimated to have outpaced Holocene rates (Karlin and Zierenberg, 1994). Sediment fill in spreading centers can act as a low-permeability barrier to advective heat extraction, whereas interbedded basaltic sills and turbidite sediments may be considerably more permeable (10^{-16} to 10^{-17} m^2 for shallow sediments versus $\leq 10^{-12}$ m^2 for deeper units) (Davis and Fisher, 1994).

Previous surveys of Escanaba Trough suggest that steep-sided sediment hills hosting massive sulfide chimneys and mounds at their margins result from basaltic sills intruding into the sediment (Fouquet et al., 1998; Clague et al., 2022). There are igneous intrusions occurring throughout the Escanaba Trough, generally divided into two primary regions NESCA, or northern Escanaba, and SESCA, or southern Escanaba. Similar igneous intrusions in Middle Valley and Guaymas Basin have been proposed to act as conduits for hydrothermal fluid flow to the seabed (e.g., Einsele et al., 1980; Lonsdale and Becker, 1985; Davis and Villinger, 1992; Davis and Fisher, 1994). The western slope of Central Hill, which occurs with in the NESCA region, (located at TN403 dive 1418 and ODP Hole 1038) hosts the most extensive sulfide mineralization observed at Escanaba Trough during Ocean Drilling Program Leg 169 (Fouquet et al., 1998). In total, 262 hydrothermal chimneys have been counted using

AUV-based maps in proximity to uplifted sediment hills in Escanaba Trough (Clague et al., 2022).

Sulfide minerals precipitated from hydrothermal fluid may preserve the isotopic profile of the material altered by hydrothermal fluid, whether bare rock or sediment. Escanaba Trough sediment fill has a higher proportion of ^{207}Pb and ^{206}Pb relative to ^{204}Pb compared to nearby Gorda Ridge basalt. Escanaba Trough sulfide has a similar Pb isotope composition to sediment, whereas Middle Valley sulfide is intermediate between sediment and basalt (Fouquet et al., 1998). These findings suggest that metal cations in hydrothermal sulfides at Escanaba Trough are derived largely from sediment fill.

In late spring of 2022, a USGS-led research team returned to Escanaba Trough during an expedition on the R/V *Thomas G. Thompson* (TN-403) and collected push cores and rock samples using the ROV *Jason*. Push cores ≤60 cm long were taken in transects extending from sulfide outcrops to “background” sediment in order to establish a gradient of hydrothermal characteristics, helping to define the extent of influence of each vent site on seafloor and shallow materials. Background sediment was collected to help characterize reference (non-hydrothermal) conditions, where there were no obvious signs of interaction with the proximate hydrothermal system, such as sulfide rubble, Fe-oxide staining, vent fauna, or diffuse flow. Understanding the physical, geochemical, and mineralogical changes associated with the transition from areas of active venting to areas of pelagic and terrigenous sediment is crucial for resolving the extent of high temperature hydrothermal mineralization in Escanaba Trough.

This paper focuses on the observed physical, geochemical, and mineralogical characteristics of push core samples collected from southern Escanaba Trough (Figure 1B). The primary physical characteristics of interest are (a) CT intensity, evaluated as a proxy for density, and (b) gamma-gamma density, a quantitative measure of density. Europium concentrations relative to other rare earth element and yttrium concentrations (REY), as well as Fe as a proportion of total Fe, Al, and Mn, are used as geochemical proxies for indicating hydrothermal influence. Principal component analysis (PCA) of XRD spectra is used to bin samples with similar mineralogy. Analytical methods used throughout this paper will be refined for future studies. These methods will be used to determine how the characterization of shallow materials both proximal and distal to sites of hydrothermal venting can be used to determine the extent of hydrothermal influence on the surrounding seabed. Or more simply, what is the footprint of a hydrothermal vent site on the seabed?

2 Methods

2.1 At Sea

New cores and data were collected during expedition TN-403 on the R/V *Thomas G. Thompson* with the ROV *Jason* and AUV *Sentry* in May-June 2022. Gravity cores up to 4.5 m in length were collected using the ship's A-frame while stationed above areas of interest. Sediment push cores were collected with *Jason* from sediment hills identified on maps created using autonomous underwater vehicles, two Dorado-class AUVs (Clague et al., 2022) and *Sentry* (during TN-403). Push cores were 9 to 59 cm long and were taken along transects extending from areas of massive sulfide outcrop to areas dominated by background sediment (Figure 2). Vent sites were visually identified as regions with accumulations of hydrothermal minerals. Vent sites with hydrothermal fluid flow (J2-1418, Central Hill and J2-1421, S3) were classified as "active" while the sites that lacked active fluid flow were termed "inactive" (Jamieson and Gartman, 2020) (Table 1). Upon shipboard recovery, cores were capped and stored vertically at 4°C to slow the oxidation of any metal sulfides in the sediment.

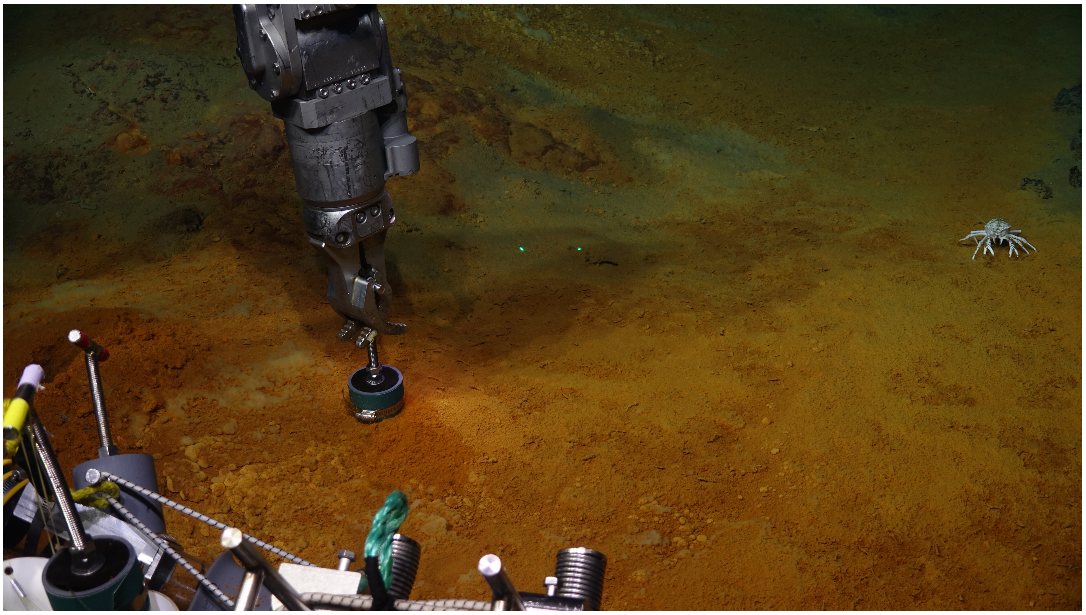

Figure 2. Push core being collected with ROV Jason during TN-403 to southern Escanaba Trough.

Rock samples were collected from rock outcrops and hydrothermal chimneys using the manipulator arms of the ROV *Jason*. Recovered rock samples were stored at -20°C to slow the oxidation of metal sulfides in the rocks.

2.2 Lab Analyses

After returning to shore, sediment cores were CT scanned using a GeoTek rotating X-ray and computed tomography core logger. The CT scans were collected using an operating voltage of 130 kilovolts (kV) and a current of 325 milliamperes (mA). The cores were split after CT scanning using a GeoTek core splitter. One-half of the split cores were imaged using a GeoTek multi-sensor core logger (MSCL), logged using X-ray fluorescence at 1-3 cm intervals, and archived at the USGS Pacific Coastal and Marine Science Center, where they were stored at 4°C when not being analyzed or subsampled. The remaining half of the split cores were sub-sampled in regions of visually distinct strata.

Powdered rock and sediment subsamples were analyzed using X-ray diffractometry with a Panalytical X'PERT3 POWDER XRD using a Cu Kα source. Scans were collected at 40 kV and 45 mA from 5-70 degrees 2θ at a 0, -1, and +1 degree wobble, with final scans an average of these three.

Samples were analyzed for major, minor and trace elements by Activation Laboratories, Canada using multiple techniques. For subsamples without sulfide minerals, most elements were analyzed by borate fusion XRF or lithium metaborate fusion followed by inductively-coupled plasma mass spectrometry (ICP-MS) or atomic emission spectroscopy (AES). For samples containing sulfide minerals, elements concentrations were obtained using sodium peroxide fusion (FUS-Na2O2) followed by ICP-MS or instrumental neutron activation analysis (INAA). Lanthanides were normalized using post-Archean Australian shale (PAAS) values from Taylor and MacLennan (1995) and plotted to observe anomalous lanthanide concentrations. Europium anomalies were calculated to estimate hydrothermal vent input into the sediments using the following equation (Olivarez and Owen, 1991).

$$Eu/Eu* = \log_{10}\left(\frac{2 \times \frac{Eu}{1.08}}{\frac{Sm}{5.55} + \frac{Gd}{4.66}}\right)$$

CT data were processed using a Histogram Cluster Analysis Procedure (HICAP) to find CT intensity values that corresponded to different materials present in the cores (Narendra and Goldberg, 1977). A kernel density estimate (KDE) of CT intensity values mapped to a 16-bit image was created for each CT scan (Figure 3). Significant peaks were identified as being at least 1% of the maximum peak height, and clusters were bound by the valleys on either side of those significant peaks. Only areas of the KDE that were at least 0.5% of the height of the maximum peak height were used for clustering CT data. High-contrast CT images were created by selecting the lowest and highest CT values corresponding to sediments in the cores. The contrast was further enhanced by replacing the default grayscale color scheme with pseudocoloring (Figure 4).

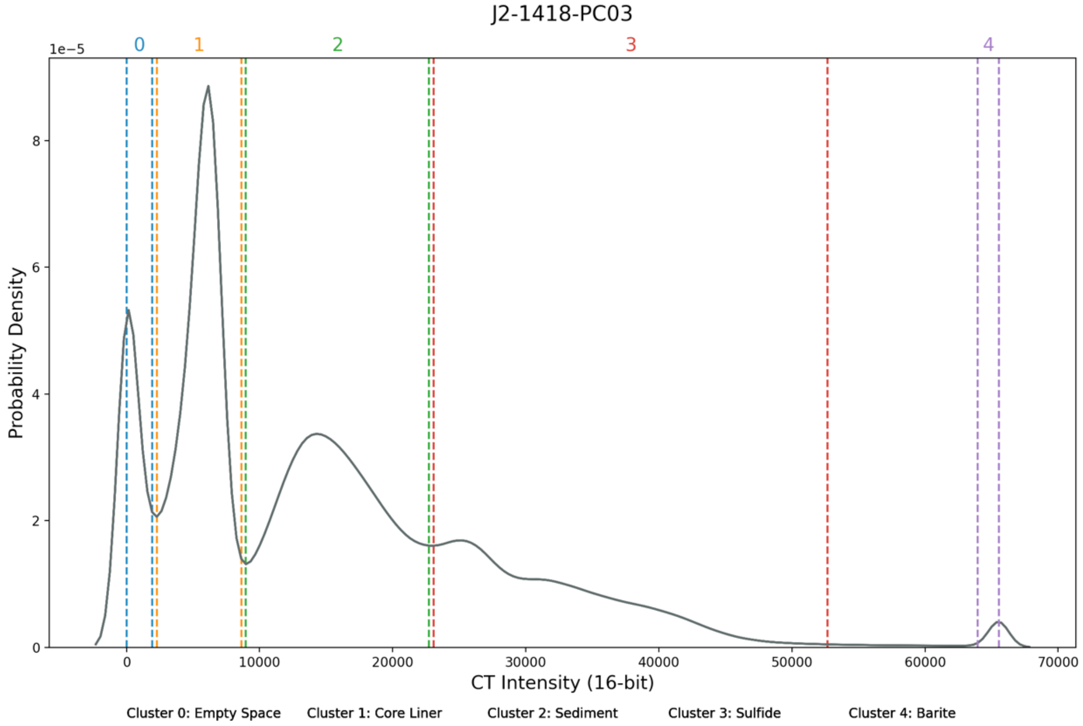

Figure 3. A kernel density estimate (KDE) of push core J2-1418-PC03 shows the method for selecting distinct CT intensity values based on material in the core. The first and last peaks are cut off because the KDE extends beyond the actual range of values in the 16-bit image (0-65536).

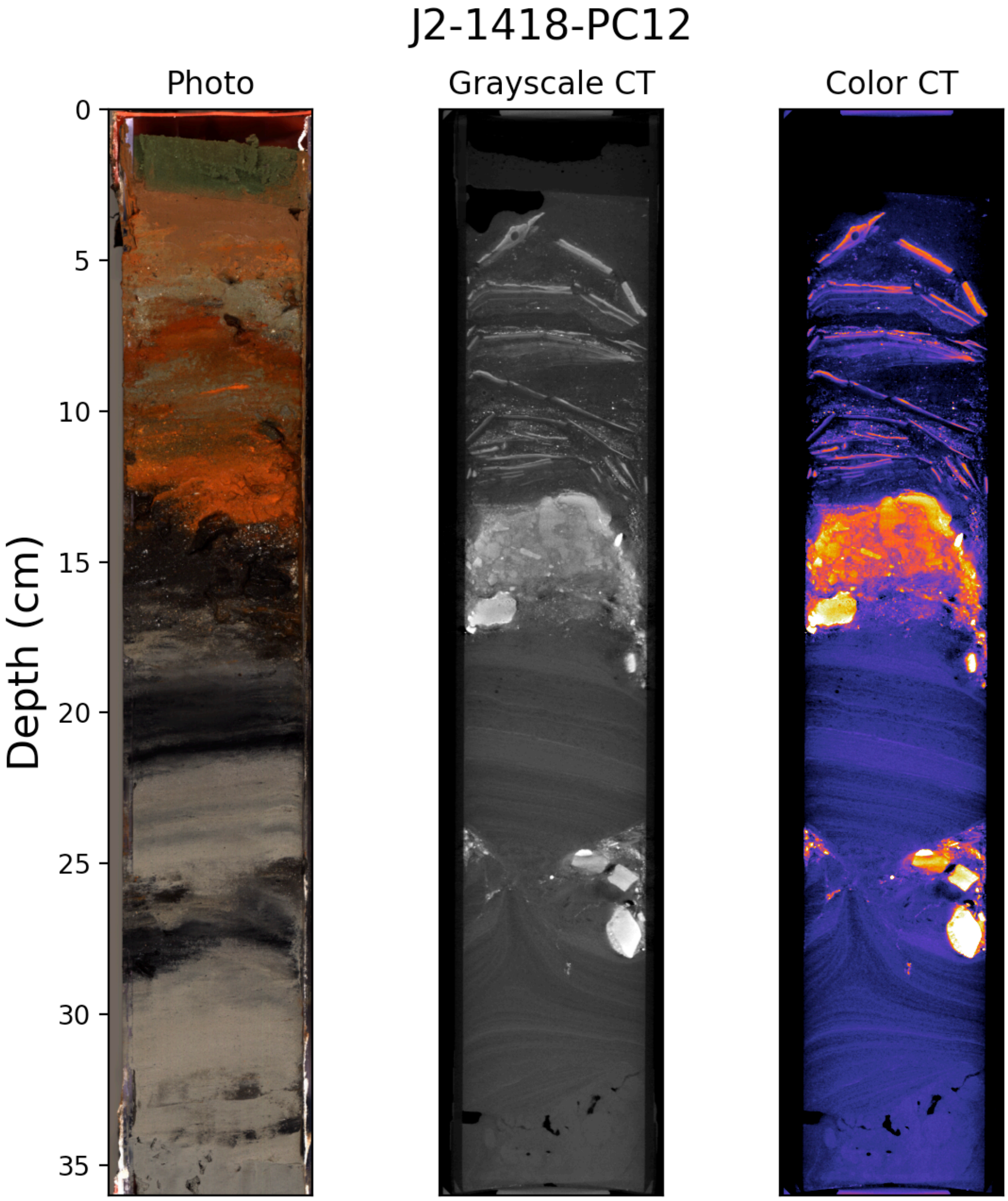

Figure 4. A photo, grayscale CT image, and pseudocolored CT image for push core PC12 from Dive 1418 at Central Hill. Platy morphology of Fe-oxides is not visible in the photo but is apparent in the grayscale CT image and further highlighted with pseudocoloring.

Because hydrothermal minerals in Escanaba Trough have a higher density than the sediment fill, CT intensity values can be used to differentiate sulfide and rocky iron oxide material from background sediment. CT intensity values associated with sulfide minerals and rocky iron oxides can be used to map the distribution of hydrothermal material across the push cores taken at each dive site. CT intensity values for push cores farthest from the hydrothermal mound are considered to represent the background end member of each dive and were used to map the distribution of background sediment across all the push cores from each dive.

Mass balance estimates for sulfide in the cores were derived from counts of CT intensity values above the background threshold value as a percent of total sediment CT intensity values. Estimates for background material in the cores were derived from CT intensity values corresponding to sediment in the background end-member core J2-1418-PC15. CT intensity values were taken from an average of two perpendicular slices of each core to provide a rough estimate of material volume.

Grain-size analyses were conducted using chemical and physical methods. Samples were subsampled (~10 g) and soaked in 10 mL of 30% hydrogen peroxide overnight to remove organics. Excess hydrogen peroxide was removed by heating subsamples to 250°C. Subsamples were sonicated to separate silt and clay from larger sediment grains. Centrifugation rinsing was used to remove soluble material. Wet sieving with a 1mm sieve was used to remove gravel, and clay was separated using a 0.063mm sieve. Coarse sand (2mm - 1mm) and sand (1mm – 0.063mm) were also separated by wet sieving.

Clay mineralogy was determined by x-ray diffraction (Poppe et al., 2001). Sediment samples were oriented by filtration onto a paper filter and washed with deionized water while using a vacuum to purge excess water from the sample. The oriented material was imprinted on 0D silicon wafers for from the paper filters for XRD. The four treatments of oriented samples were: 1. Oriented samples without further alteration; 2. Glycolated samples using ethylene glycol to expand any swelling clays 3. Heated samples, which were to 400°C for 30 minutes and 4. Heated again to 550°C for 30 minutes. Samples were X-ray diffracted following each step to observe changes in mineralogy that indicate specific clay identities.

3. Results

3.1 CT

CT imaging does not provide a quantitative measure of density, but it can show density contrasts in a material. By comparing the CT results with density results obtained from gamma-gamma density measurements, which are quantitative, we demonstrated a strong positive correlation between CT intensity and density (Figure 5).

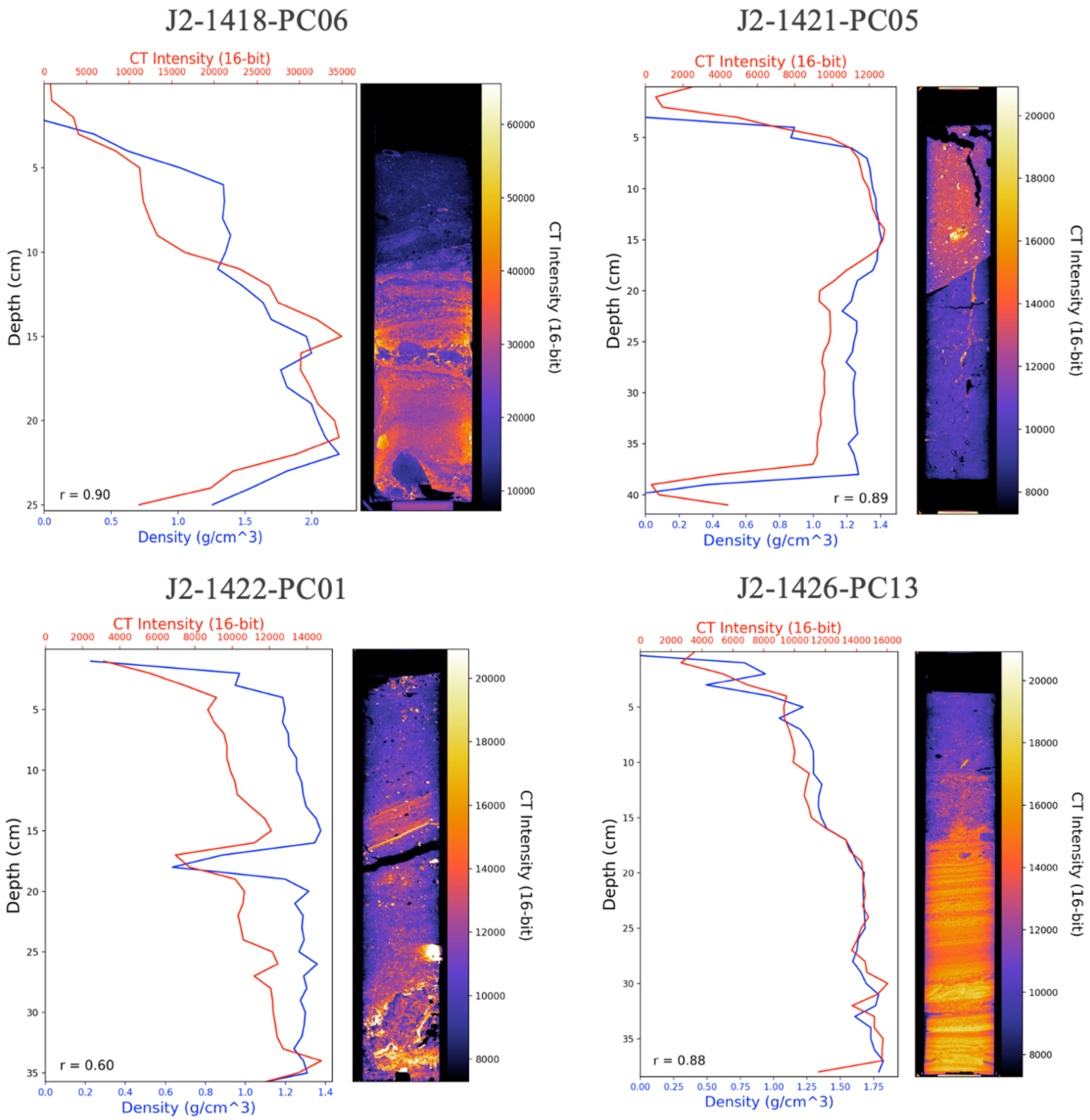

Figure 5. The correlation between CT intensity and density measured via a gamma source in push cores. Density (blue line) was measured via a gamma source.

Samples taken closest to the hydrothermal mounds represent the hydrothermal end members of the hydrothermal gradient, whereas those taken farthest away represent distal end members. CT imaging of push cores from dives with hydrothermal material shows that denser hydrothermally derived material is rocky, consisting of mass-wasted chunks of hydrothermal chimneys and mounds, and takes on one of two forms. The material is either well-preserved massive sulfide or platy iron oxide weathering products, although some disseminated rocky material is present in background sediment closer to the hydrothermal mound, as indicated by CT intensity but was not extracted and identified.

There appears to be a correlation between grain size and CT intensity. Sediments with more sand as a fraction of grains had a higher CT intensity than those with higher clay and silt fractions (Figure 6). However, grain size was only measured in 4 push core samples and of those 4 samples only 2 were from the same core. Given the small sample size for grain size, we cannot confidently say that sediment with a higher fraction of sand has a higher CT intensity.

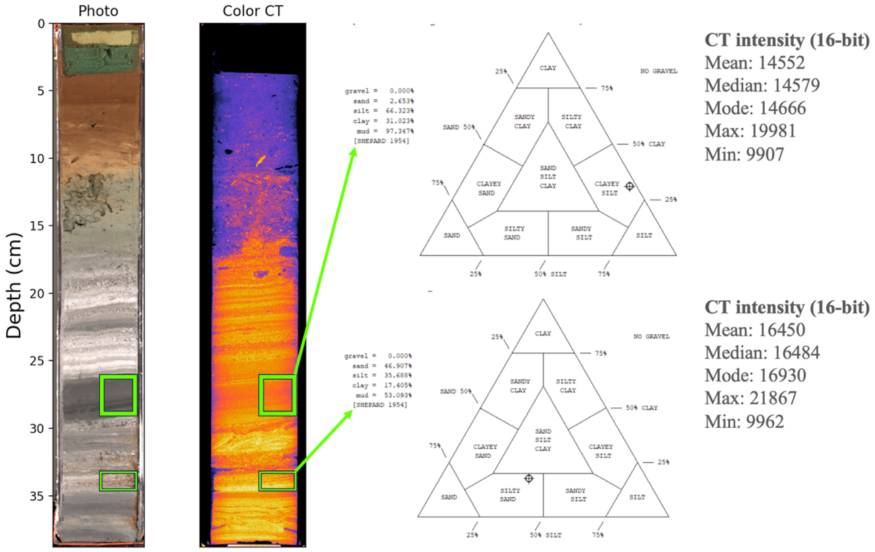

Figure 6. Grain sizes for two samples from J2-1426-PC13 are shown with their respective summary statistics of CT intensity.

Of the seven dives that recovered push cores, dive 1418, located at Central Hill, recovered five cores with sulfide mineralization and one core without any obvious hydrothermal material (Figure 7). The core without hydrothermal material is the core recovered farthest from the hydrothermal mound and is used as the background end member for the hydrothermal system at Central Hill.

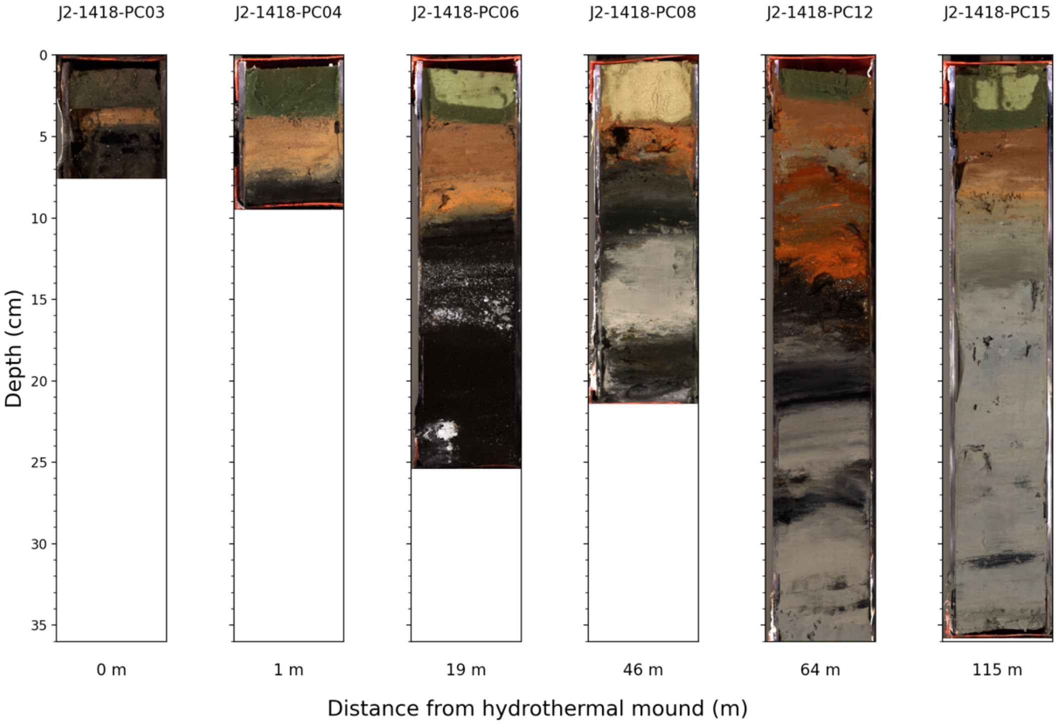

Figure 7. Linescan images of the six cores recovered from dive 1418 at Central Hill, Escanaba Trough. Distance from the edge of the hydrothermal mound is labeled in meters at the bottom of each core.

The highest point on Central Hill is 125 m above the surrounding seafloor, with a depth to the top of the underlying sill of 404 m (Clague et al., 2022). The lateral dimensions of Central Hill are 2.4 x 1.6 km (long x short axis), with the long axis striking North-South. The laccolith that uplifted Central Hill is estimated to have intruded between 450 – 1685 years ago based on sediment accumulation rates (Clague et al., 2022).

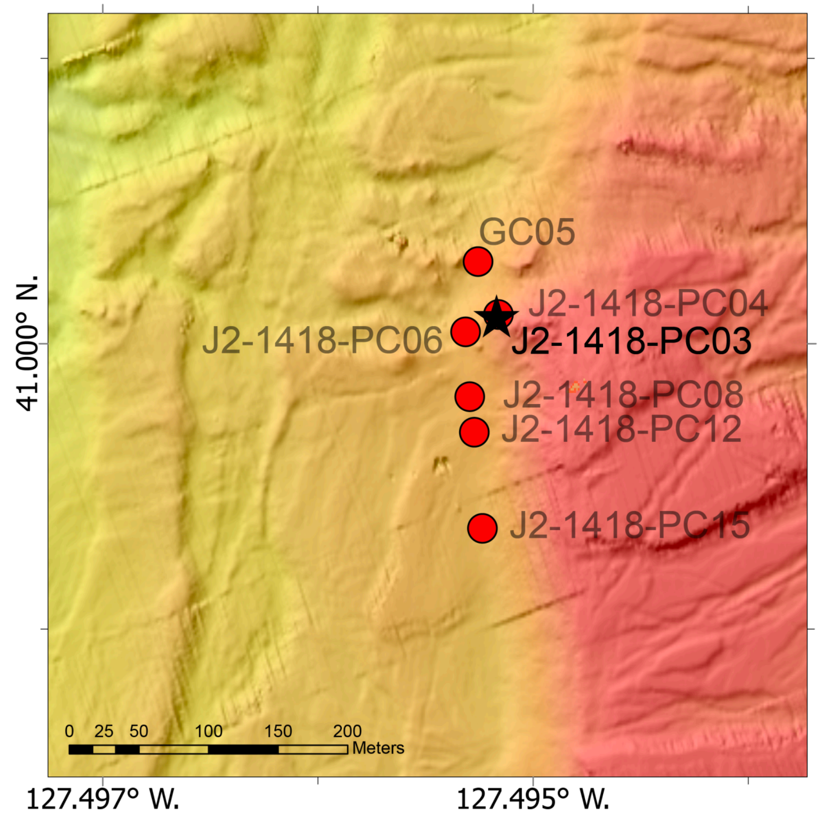

Figure 8. The location of each push core taken during dive 1418. GC05 is a gravity core not discussed in this thesis. Central Hill is the red region on right side of the map. The star represents the sample taken closest to the vent site (from Manda Au, USGS).

In any CT scan of a push core, there were discrete peaks in the KDE associated with distinct materials. The empty space at the margins of the CT scan and any air pockets in the core have CT intensity values of 0, leading to a large distinct peak in the KDE at a CT intensity of 0 (Cluster 0 in Figure 3). Moving along the KDE, the next peak occurs between CT intensity values of 2000 and 8000, corresponding to the plastic core liner and flower foam used to pack the cores for transport (Cluster 1 in Figure 3). The silicate sediment that fills Escanaba Trough has

CT intensity values between 8000 and 20000 (Cluster 2 in Figure 3). Rocky sulfide and Fe-oxide material have CT intensity values between 20000 and 50000 (Cluster 3 in Figure 3). A few cores have small peaks in their KDE at 65536, which is the maximum CT intensity value for our 16-bit images. Push core J2-1418-PC03 illustrates that small pieces of material cause the maximum intensity peak (Cluster 4 in Figure 3).

The origin of the small grains, which result in the maximum intensity peaks in J2-1418-PC03, is uncertain, and they don't match the thin streaking associated with noise (Boas and Fleischmann, 2012). No minerals with densities much greater than the sulfide minerals were identified in samples from Escanaba Trough. Barite was identified as a minor component of the upper section of core J2-1418-PC03 using XRD. Barite is often associated with hydrothermal vent settings and was identified in multiple samples (Table 2 and geochemistry results, next section; Griffith and Paytan, 2012). Barite displays strong radiopacity and is used in medical settings to provide high contrast in CT scans (American College of Radiology, 2023).

A core tube loaded with mineral standards of Escanaba sediment, massive pyrite, crushed pyrite, and barite was used to determine CT intensity ranges for minerals found at Escanaba Trough (Figure 9). The highest CT intensity values corresponded to tabular barite crystals within the standard core due to the radiopacity, as barite has a lower density than pyrite. In addition to density-based discrimination, CT scanning could potentially be used to determine the location and distribution of barite in our push cores by locating areas with CT intensity values at the upper end of the measured range.

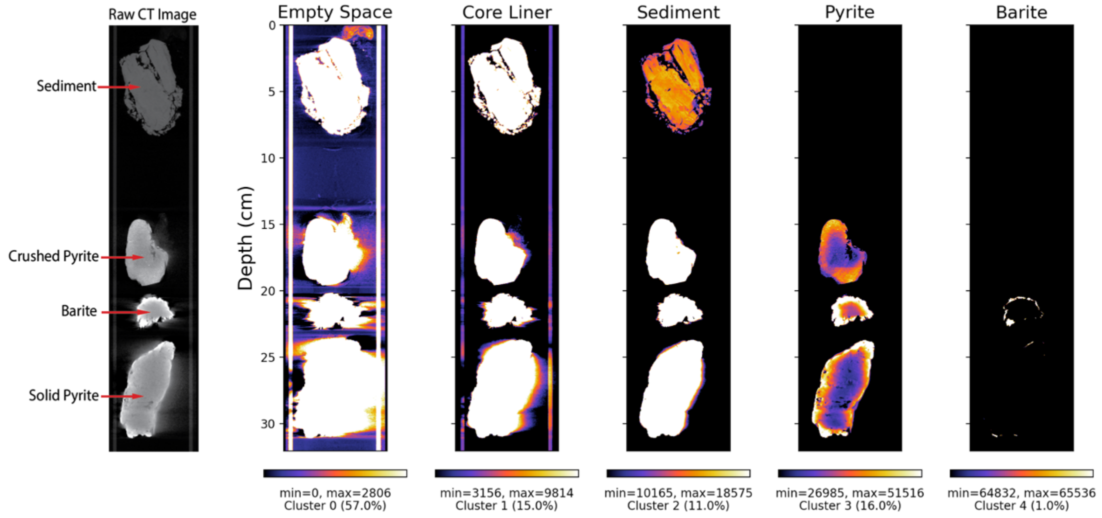

Figure 9. Materials in the standard core are highlighted based on their CT intensities. For figures 8 and 9, to clearly illustrate the clusters a narrow range of intensities is in range (range at bottom of image). Intensities less dense than the highlighted cluster are shown in black; intensities more dense than the highlighted cluster are shown in white. The highlighted material is named at the top of each image (L-R- empty space, core liner, sediment, pyrite, and barite).

The volume of sediment or hydrothermal material in a core can be estimated using the CT images and HICAP clustering. Because the first two clusters in the KDE of the CT image correspond to empty space and plastic liner, the remaining clusters correspond to the actual sediment recovered in the core (Figure 10). The percentages shown under each cluster in Figure 10 are the percent of pixels in the CT image that fall into those bounds of CT intensities. Each slice yields estimates for an area; for example, 34% of the area of the CT image for push core J2-1418-PC03 has intensity values that fall into the range of Cluster 2. To estimate volume, at least 2 slices are needed.

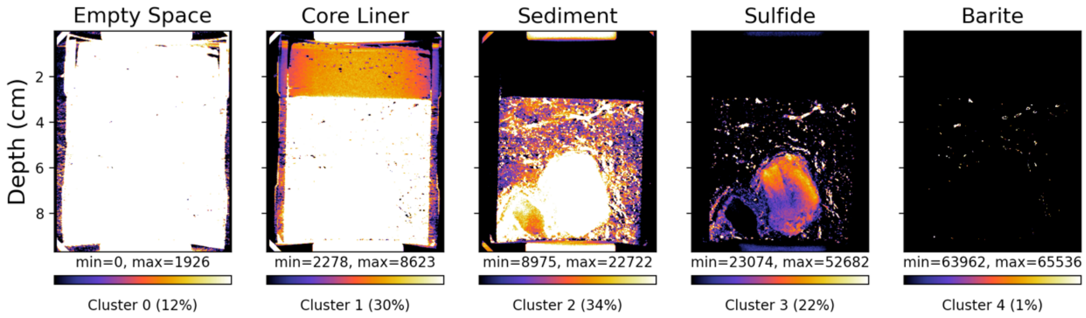

Figure 10. Results of CT image segmentation using a HICAP shown on push core J2-1418-PC03 from Central Hill, Escanaba Trough. Foam and plastic core tubing are clearly delineated in Cluster 1. For figures 8 and 9, to clearly illustrate the clusters a narrow range of intensities is in range (range at bottom of image). Intensities less dense than the highlighted cluster are shown in black; intensities more dense than the highlighted cluster are shown in white.

For samples from dive 1418 at Central Hill, massive sulfide is the predominant material in the lower portion of push cores J2-1418-PC03, J2-1418-PC04, and J2-1418-PC06 as determined by CT imaging, XRD, and visual identification (Figure 6, 10). In push cores J2-1418-PC08 and J2-1418-PC12, sulfide is interlayered with background sediment, suggestive of mass wasting from the hydrothermal mound (Figure 6, 10). Push cores J2-1418-PC03, J2-1418-PC04, and J2-1418-PC06 show no signs of sulfide dissolution, whereas J2-1418-PC08 and J2-1418-PC12 both have platy iron oxides overlying sulfide minerals, which could indicate regions of active dissolution. Platy accretions of iron oxide minerals adjacent to sulfide minerals appear to result from sulfide oxidation and can serve as useful indicators of regions of sulfide dissolution around vent sites (Figures 6, 10).

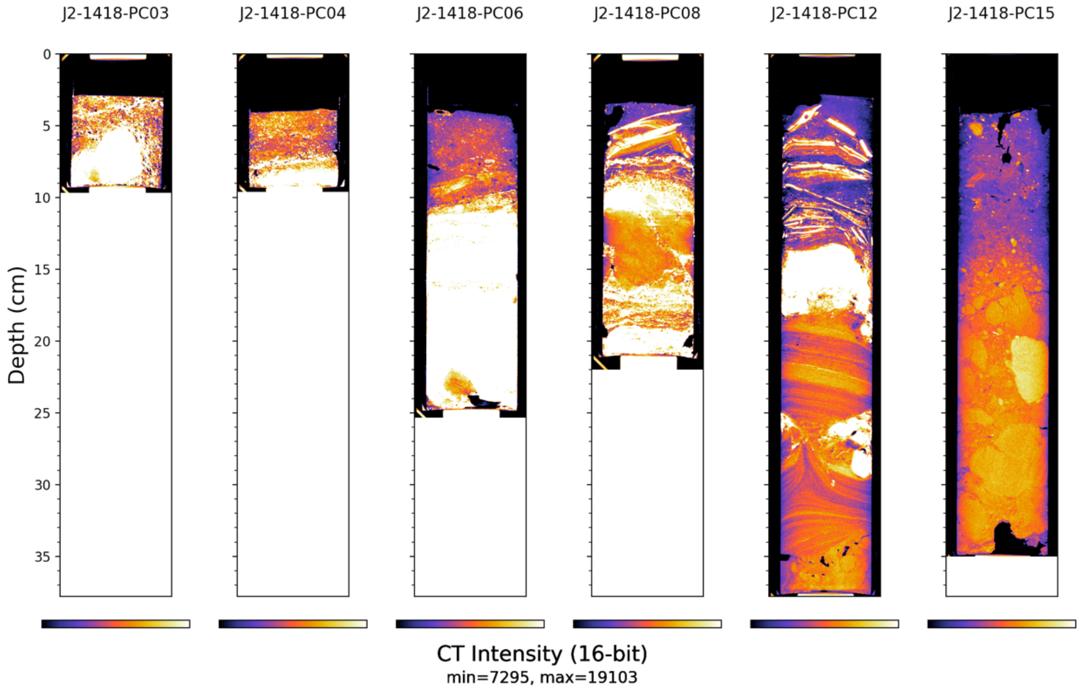

Figure 11. CT scans of the push cores from dive 1418 at Central Hill show regions of higher density in white and regions of density similar to background sediment in shades of purple and orange.

Dive 1419 (Figure 12) recovered one push core with sulfide rock and rocky Fe-oxide surrounding the sulfide rock: J2-1419-PC02. This core was taken directly at the edge of the hydrothermal mound. The platy morphology is most evident in the high-contrast CT scans of the cores (J2-1419-PC02 in Figure 12). The remaining 4 cores, which ranged between 21 and 139 m away from the edge of the hydrothermal mound and from the first core of the dive, contain no sulfide rock or Fe-oxide weathering products. The absence of these materials in cores taken beyond ~20 meters from the vent field indicates that sulfide rock may be absent or buried below ~60 cm of sediment.

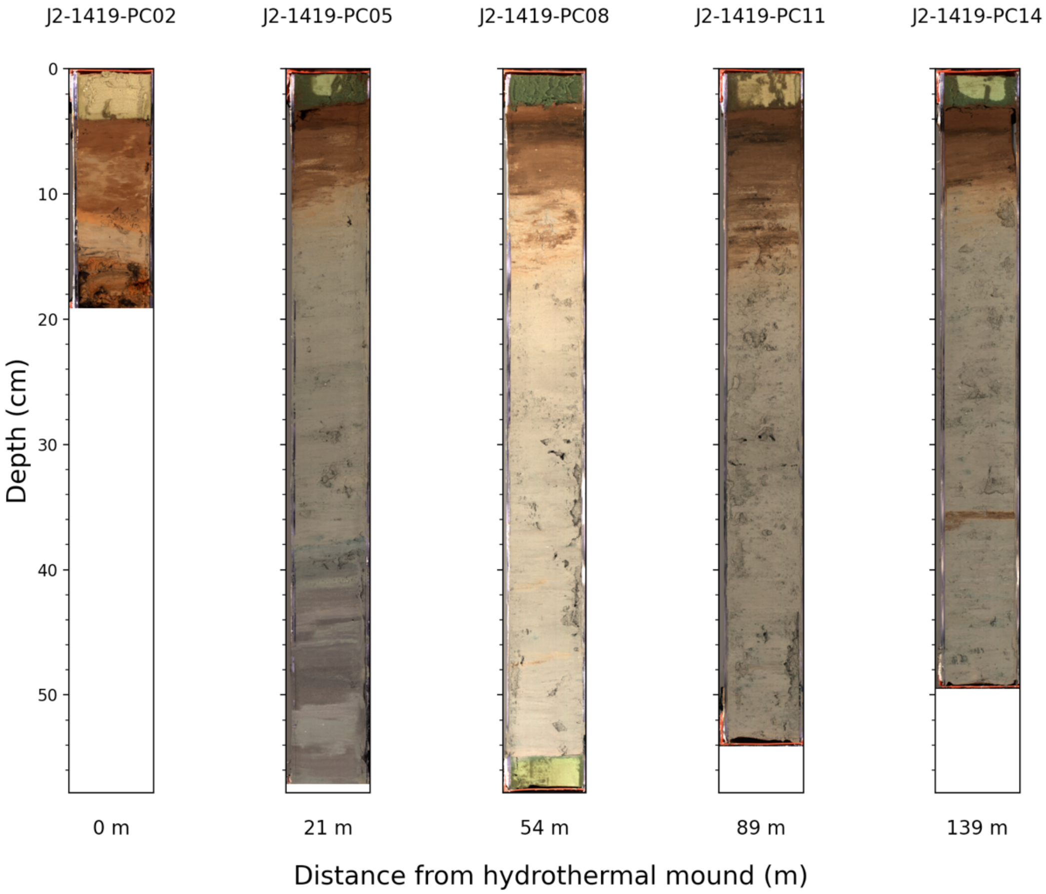

Figure 12. Linescan images of the 5 cores recovered from dive 1419.

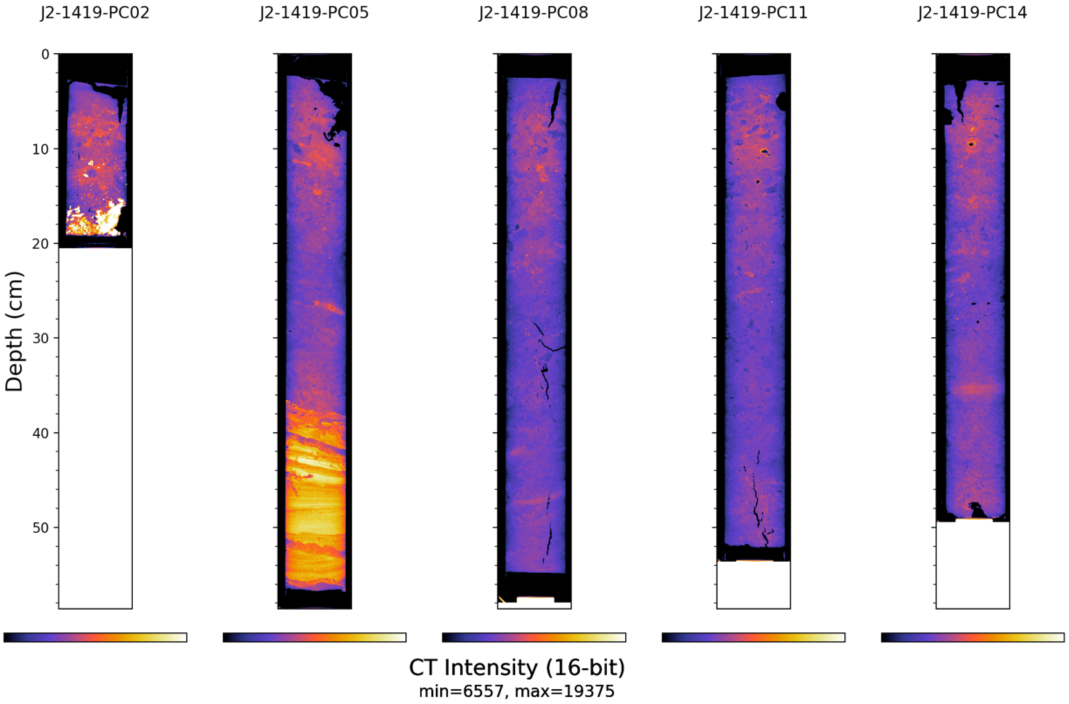

Figure 13. CT scans of the push cores recovered during dive 1419. J2-1419-PC05 was used to set the range of CT intensity to highlight the denser layer with stratigraphy at the bottom of the core.

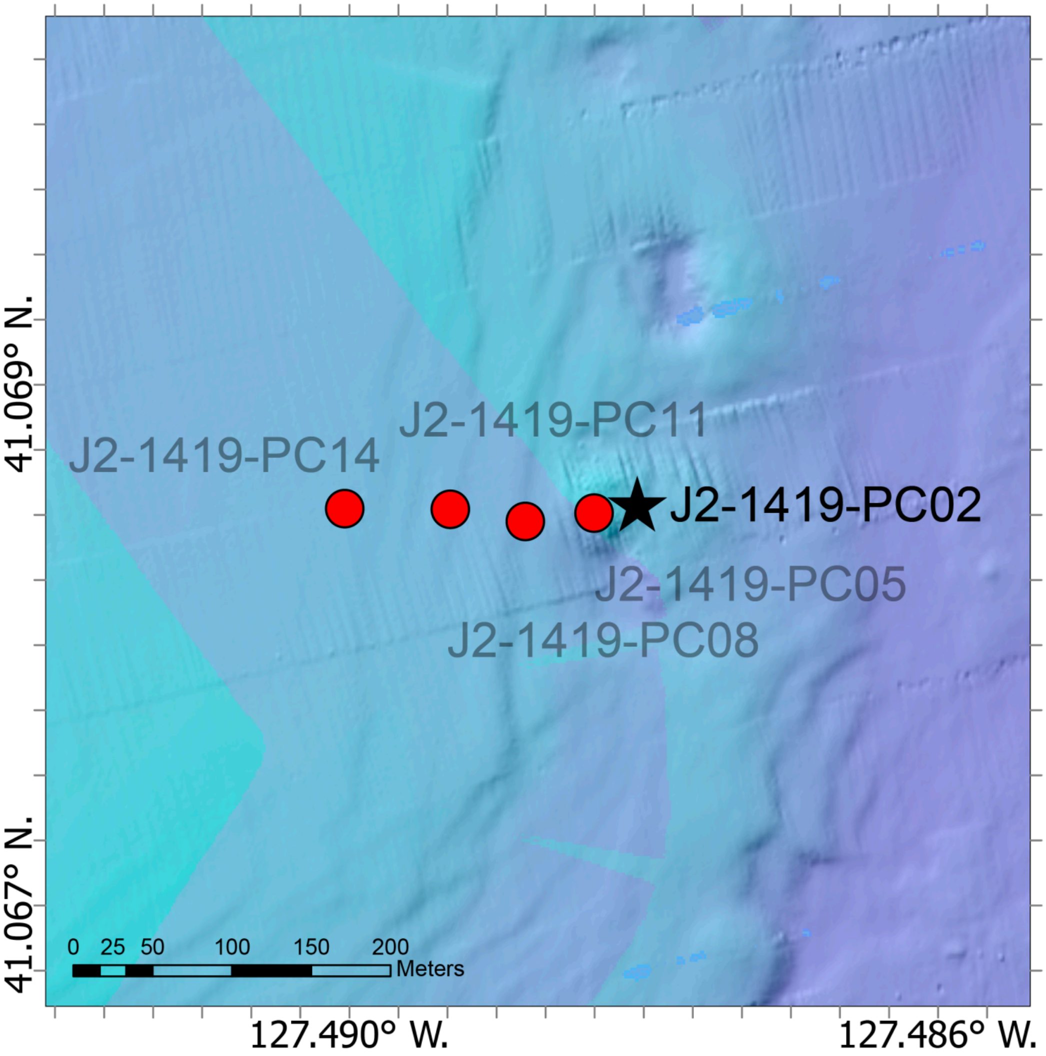

Figure 14. A map of dive 1419. The star represents the sample taken closest to the vent site (from Manda Au, USGS).

Like dive 1419, dive 1420 (Figures 15, 16, and 17) recovered one push core with platy Fe-oxide weathering products adjacent to the vent field (J2-1420-PC02 in Figure 15). The remaining cores contained no sulfide rock or platy Fe-oxides. These materials may be present > 25 meters from the edge of the vent field approximately 60 cm below the seabed, but none were recovered in push cores of that depth.

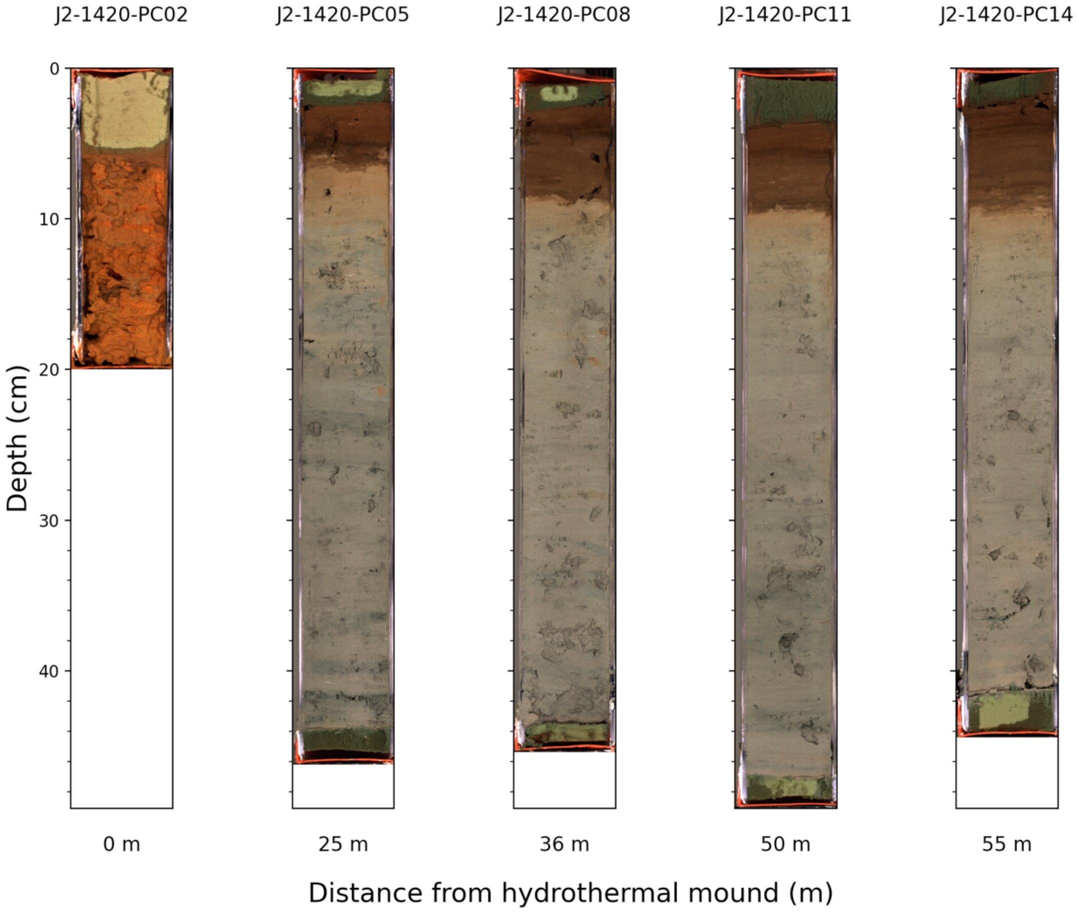

Figure 15. Linescan images of the 5 cores recovered from dive 1420.

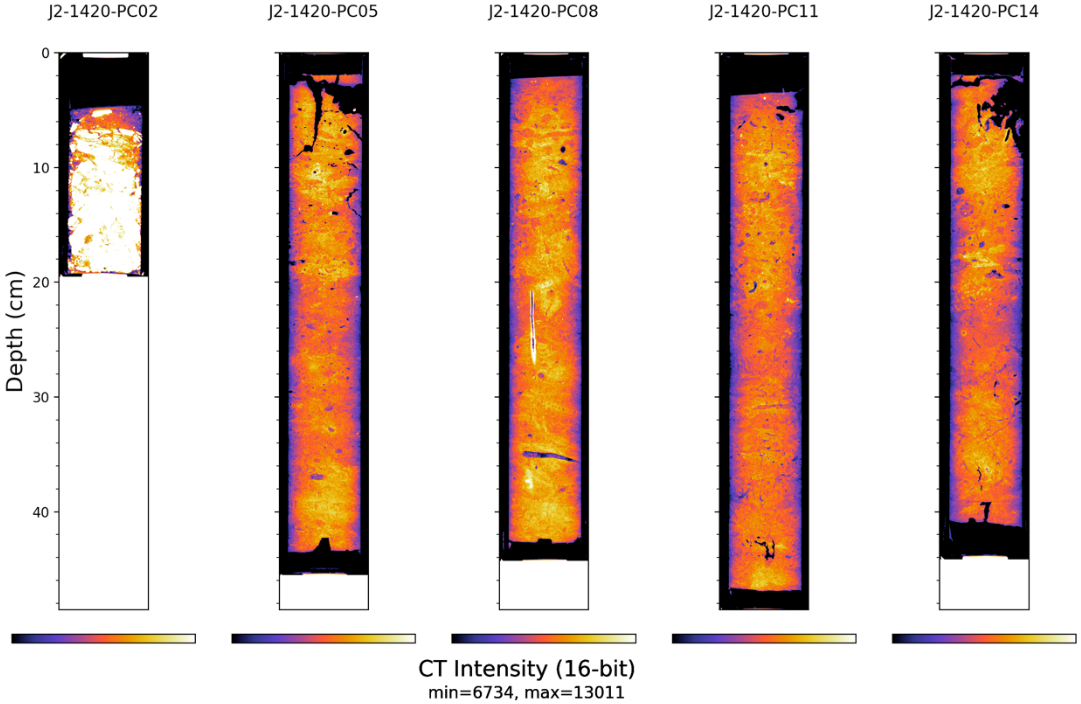

Figure 16. CT scans of the push cores recovered during dive 1420. Push core J2-1420-PC02 has denser, likely hydrothermal, material compared to the remaining cores collected farther from the hydrothermal mound.

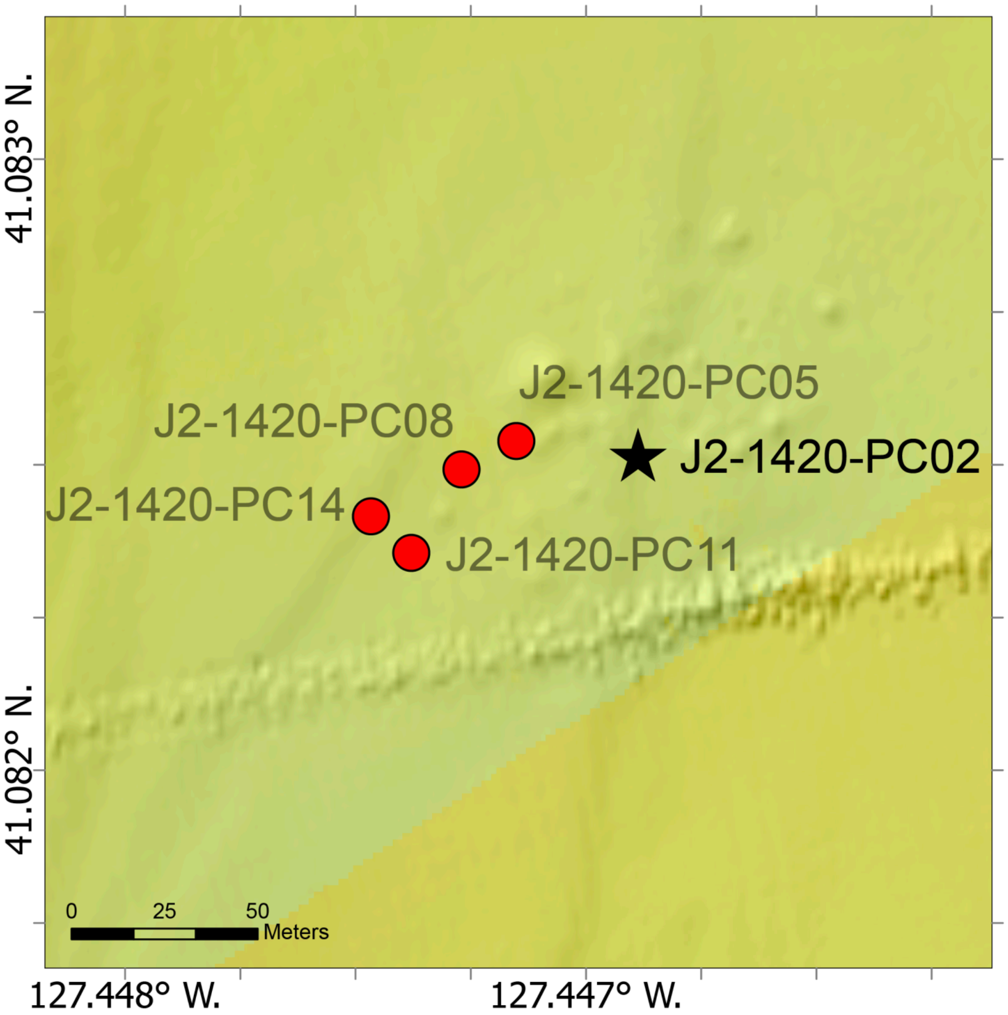

Figure 17. A map of dive 1420. The star represents the sample taken closest to the vent site (from Manda Au, USGS).

Dive 1422 recovered two cores with hydrothermal material, one adjacent to the vent site and the other approximately 20 meters away (J2-1422-PC01 and J2-1418-PC04 in Figure 18). The hydrothermal material at the bottom of push core J2-1422-PC01, taken closest to the vent site, displayed pervasive weathering and S < 1% wt. Push core J2-1422-PC04, taken approximately 11 meters from the edge of the vent field, contained unoxidized sulfide rock buried under ~20 cm of sediment. The remaining core taken > 15 meters from the vent site contained no sulfide rock or platy Fe-oxides. J2-1422-PC07 is entirely low-density, silicate-dominated sediment. J2-1422-PC10 and J2-1422-PC13 are capped by the same lower-density material but have bottom sections composed of denser gray silicate sediment (Figures 18 and 19).

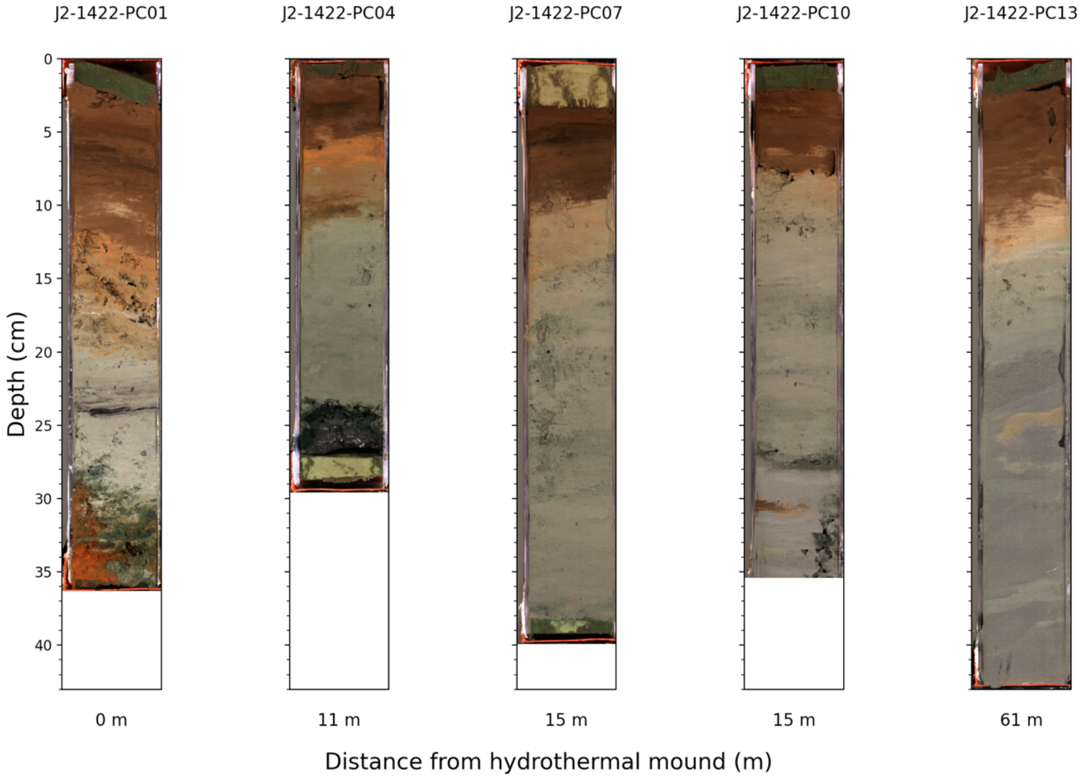

Figure 18. Linescan images of the five cores recovered from dive 1422.

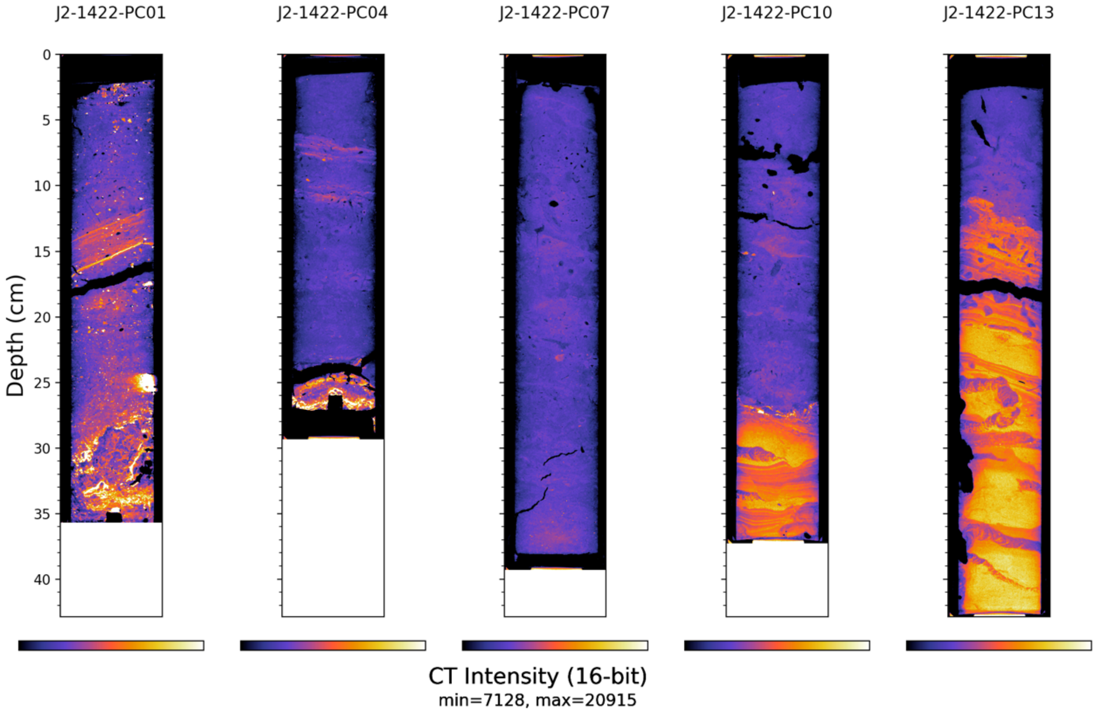

Figure 19. CT scans of the push cores recovered during dive 1422.

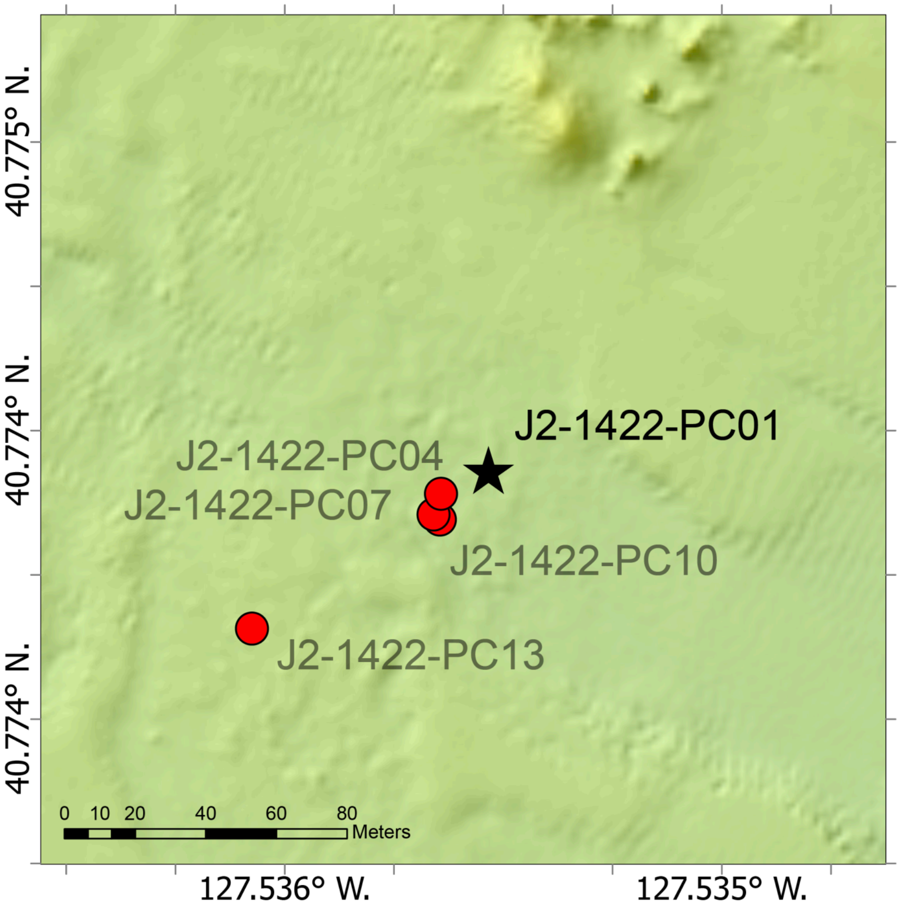

Figure 20. A map of dive 1422. The star represents the sample taken closest to the vent site (from Manda Au, USGS).

Dive 1424 recovered a 40 cm core (J2-1424-PC01) with disseminated sulfide in an approximately 10 cm thick section at the bottom of the core. The core recovered closest to the mound contained rocky Fe-oxide material (J2-1424-PC04). Core J2-1424-PC07 contained rocky material ~20 cm into the core. The final two cores taken approximately 23 and 32 meters from the hydrothermal mound, respectively, are dominated by uniform gray silt (Figures 21 and 22, J2-1424-PC10 and J2-1424-PC13).

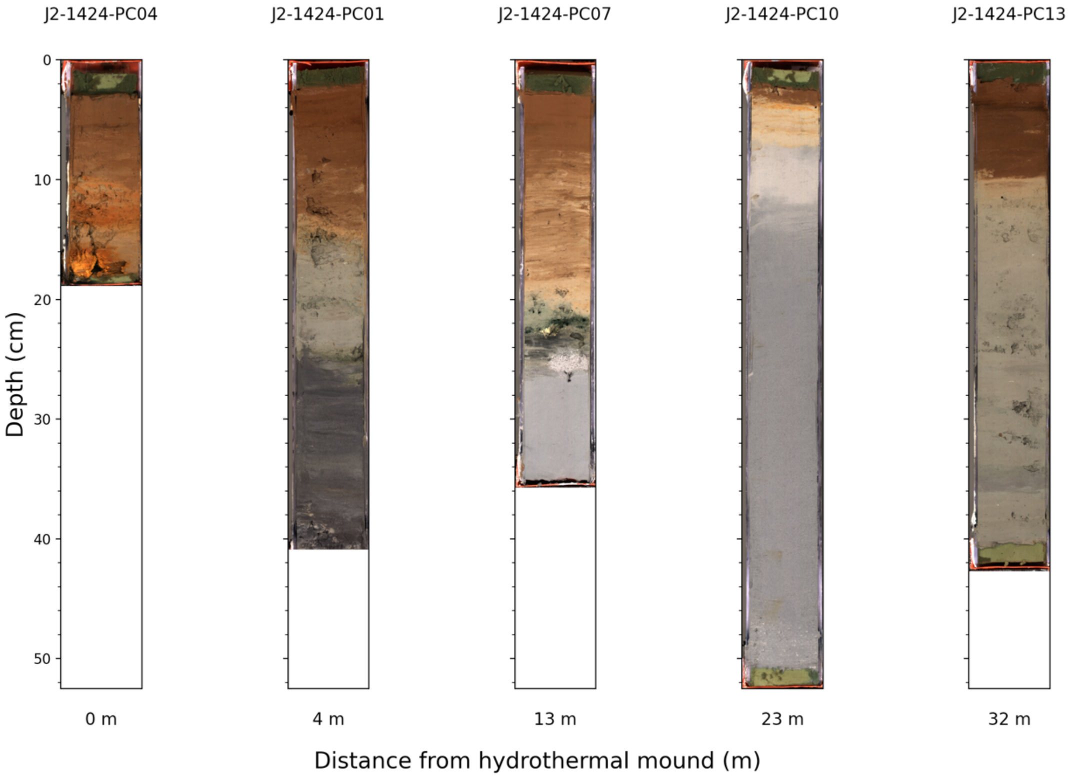

Figure 21. Linescan images of the five cores recovered from dive 1424.

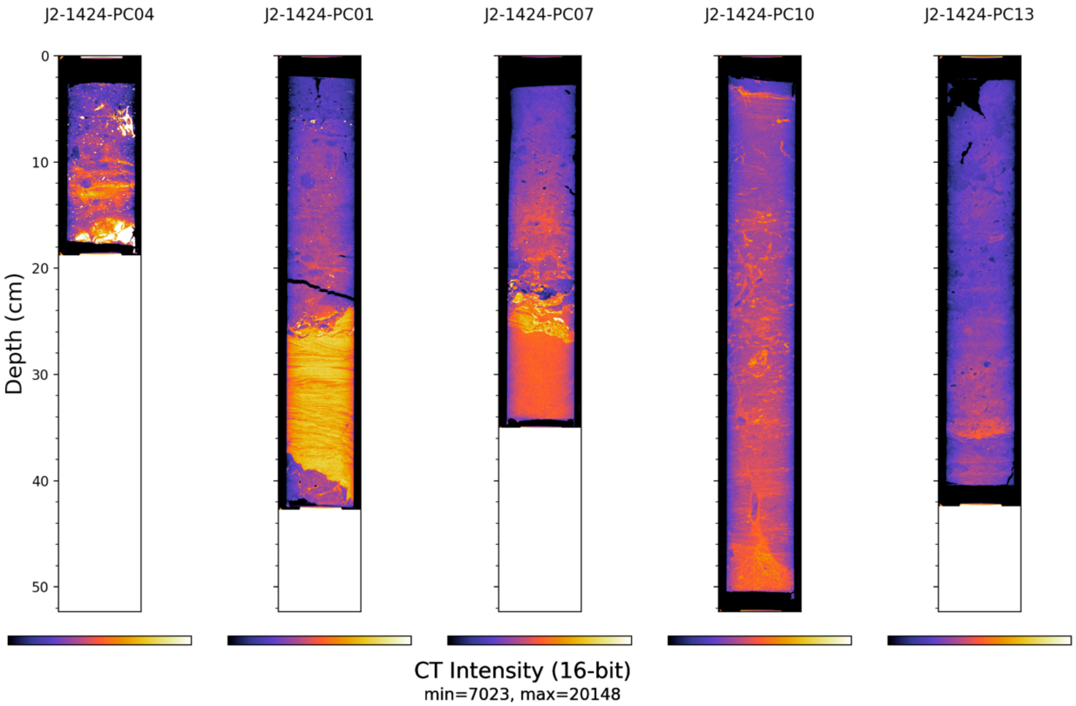

Figure 22. CT scans of the 5 cores collected during dive 1424. Hydrothermal material appears as bright regions in core J2-1424-PC04.

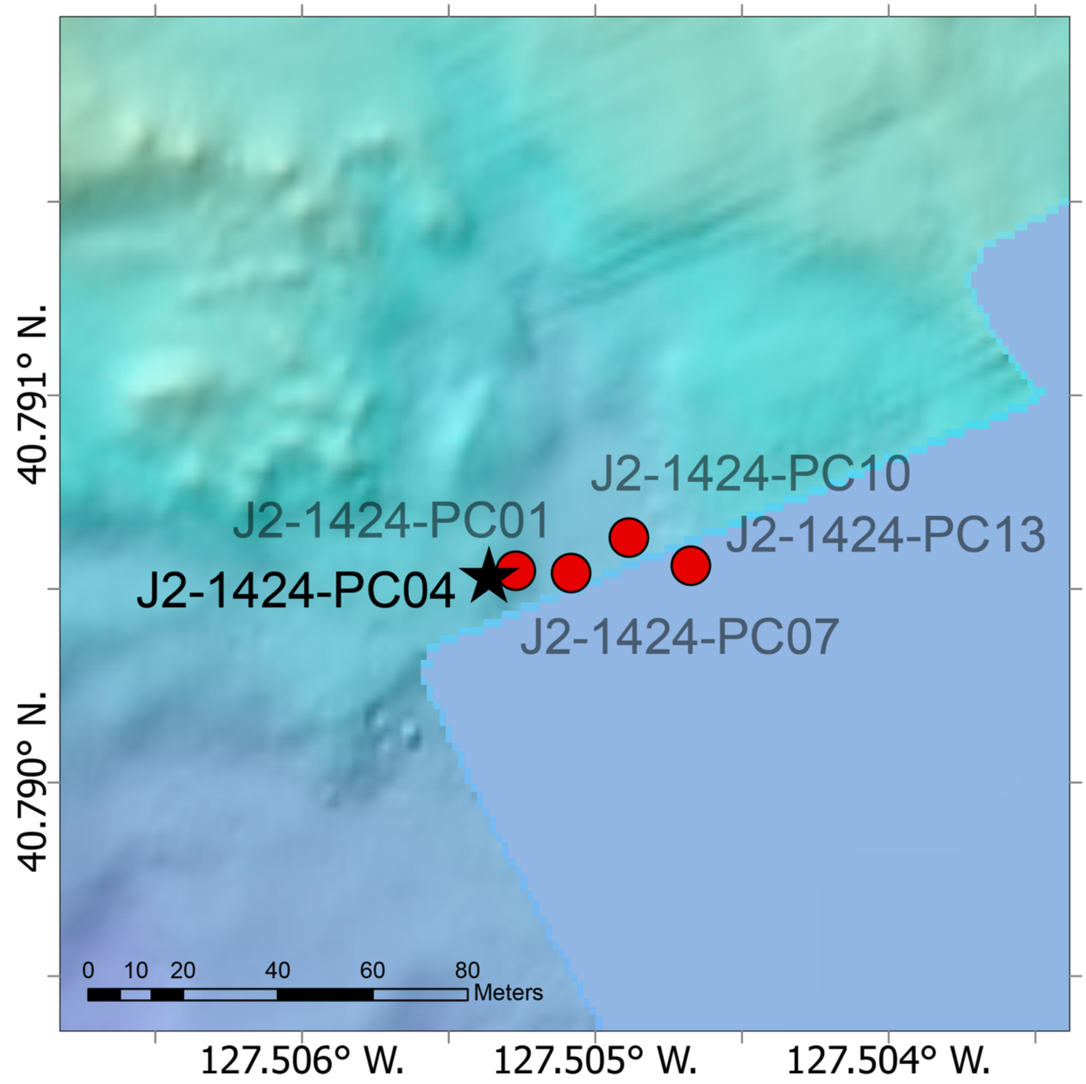

Figure 23. A map of dive 1424. The star represents the sample taken closest to the vent site (from Manda Au, USGS).

Dive 1426 recovered 5 cores (Figure 24). The first core recovered, and the core closest to the hydrothermal mound was core J2-1426-PC01. The core has a small layer of dark material that contains pyrrhotite as the primary sulfide mineral. The remaining 4 cores taken as far as 39 m from the hydrothermal mound contained no obvious hydrothermal material. Cores J2-1426-PC10 and J2-1426-PC13 have stratigraphy with high contrast in both the linescan images and CT intensity (Figure 24 and Figure 25).

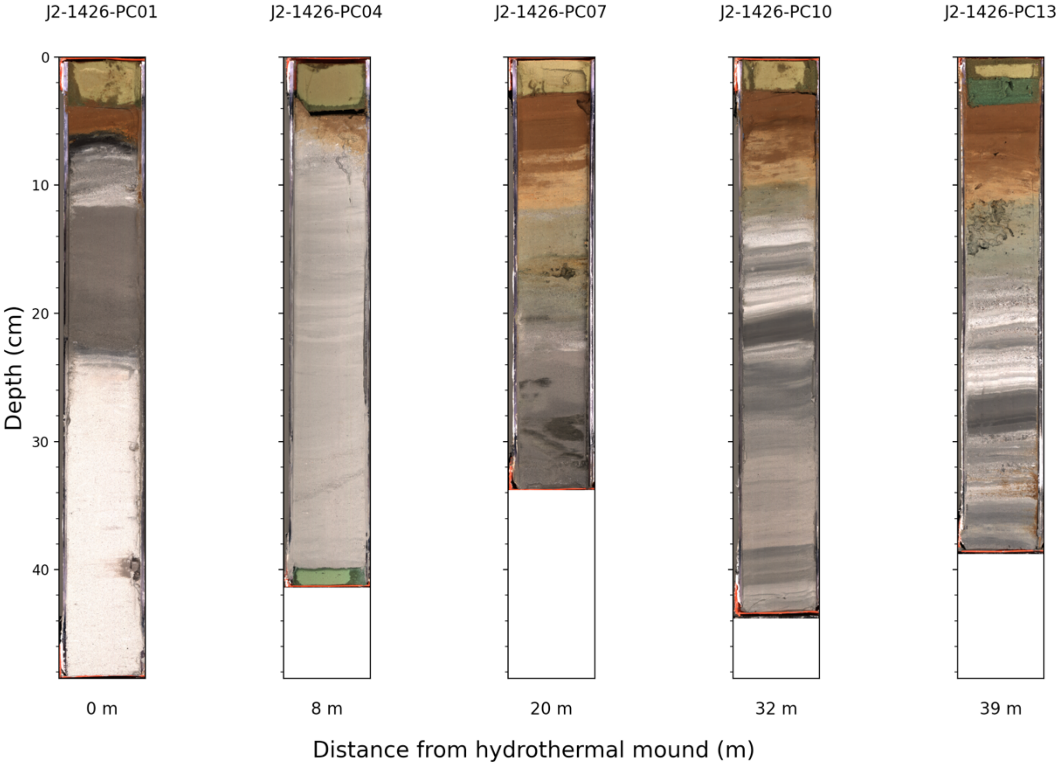

Figure 24. Linescan images of the five cores recovered from dive 1426.

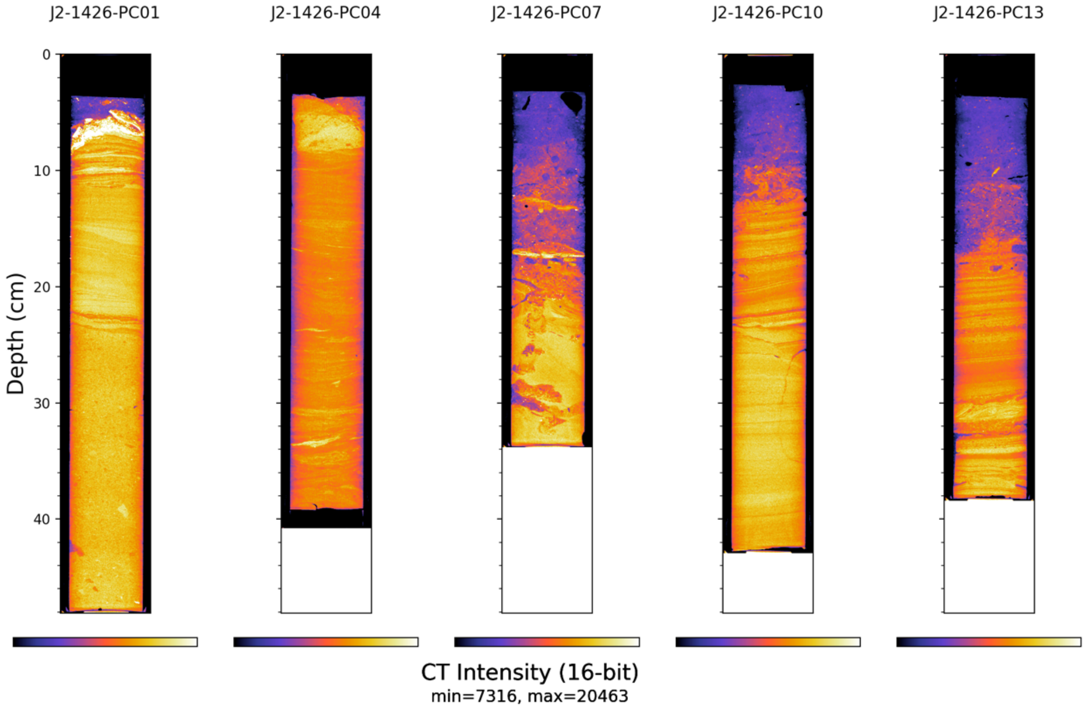

Figure 25. CT scans of the push cores recovered during dive 1426. A small layer of denser material is apparent as a bright region at the top of J2-1426-PC01.

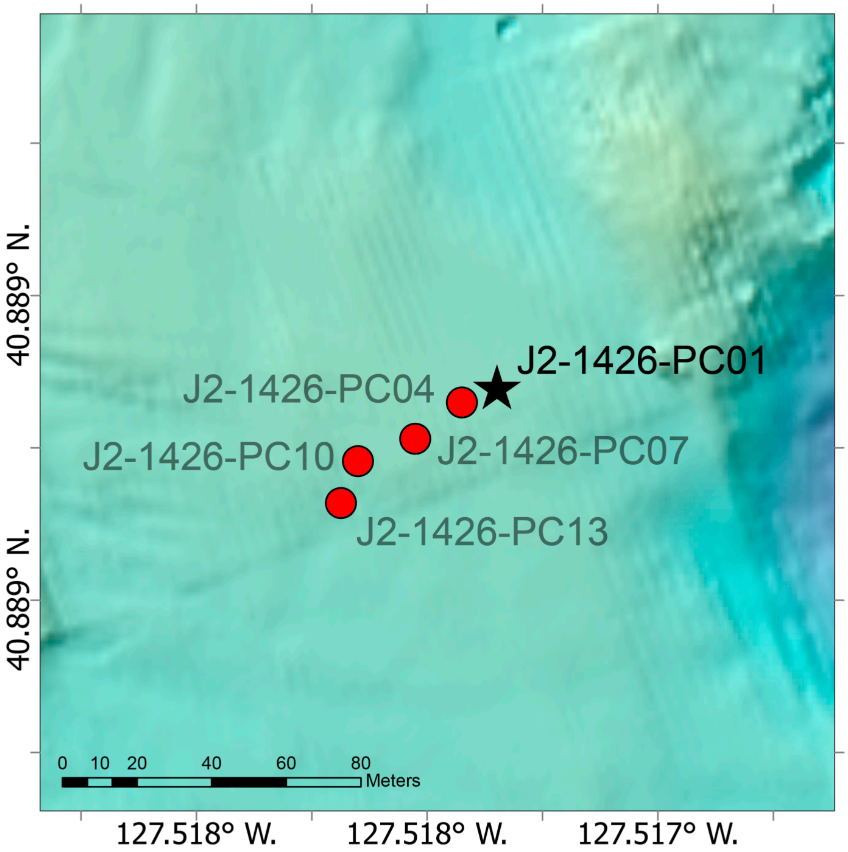

Figure 26. A map of dive 1426. The star represents the sample taken closest to the vent site (from Manda Au, USGS).

3.2 Geochemistry

Among sulfide samples from push cores, pyrrhotite and isocubanite were the primary sulfide minerals identified via XRD. Silicate sediments were primarily quartz and albite. Ferrihydrite and goethite were the most prominent Fe-oxide minerals in XRD spectra from Fe-oxide dominated samples. Chlorite was identified as the predominant clay mineral across all samples. All samples had pronounced peaks at 7Å that collapsed following heating at 550°C for 30m minutes. Peaks at ~18.8 Å and 25.1 Å associated with chlorite were also destroyed following heating at 550°C for 30 minutes. 10 Å peaks usually present in chlorite group clays at were not observed in these samples.

PCA was performed on XRD scans from all push core subsamples that also had bulk geochemistry data (n = 53). Samples were clustered based on the similarity of XRD spectra using HighScore Plus (Table 3). XRD clusters 1 and 2 represent silicate-dominated samples, clusters 4 and 5 are metal-sulfide-dominated, cluster 6 is dominated by serpentine minerals, and clusters 3 and 7 are Fe-oxide-dominated.

Geochemical ratios can also be used to classify subsamples based on hydrothermal origin. Hydrothermal origin was quantified based on the ratio of Fe to (Fe + Mn + Al). Mn and Al are relatively scarce in seafloor hydrothermal systems, so samples of hydrothermal origin will have a ratio closer to 1, with a cutoff of > 0.5 previously used (Boström, 1973; Gurvich, 2006). All sulfide and iron-oxide samples plotted towards the hydrothermal end-member, whereas silica-dominated sediments plotted closer to the background end-member (Figure 27).

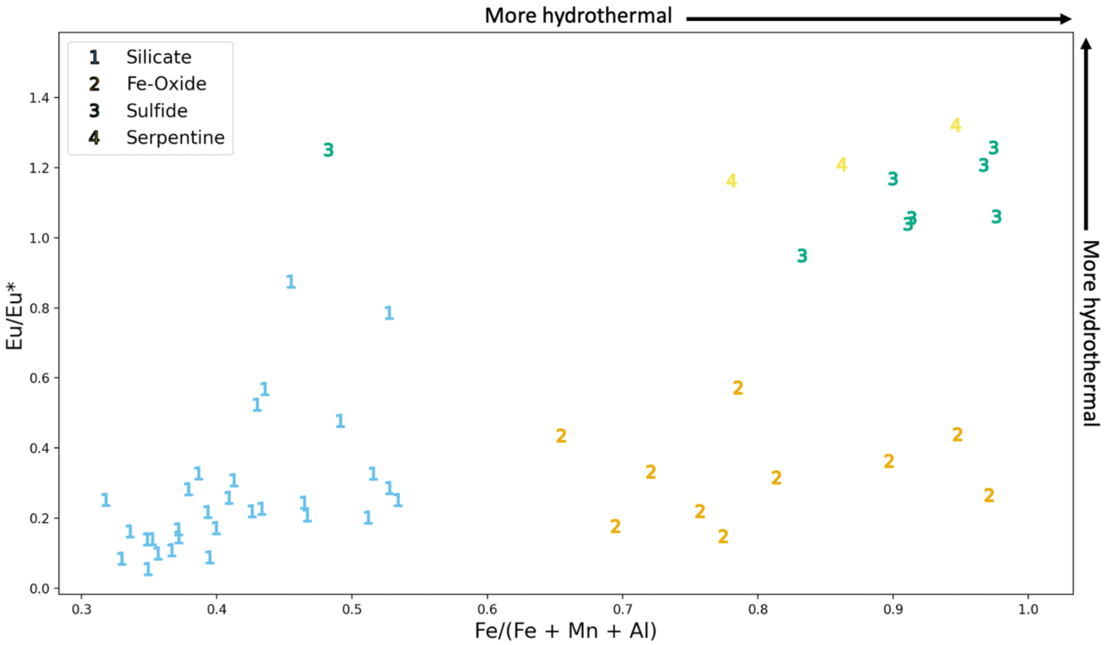

Figure 27. Samples are plotted based on mineralogy identified by XRD and bulk geochemistry. Increasing values on the X and Y axis indicate a high-temperature hydrothermal origin. XRD clusters 1 and 2 are silicate dominated sediments combined into 1 on the plot, XRD clusters 3 and 7 are Fe-oxide dominated combined into group 2, XRD clusters 4 and 5 are sulfide dominated combined into group 3, and cluster 6 is dominated by serpentine minerals shown on the plot as group 4 (XRD clusters are found in Table 3).

Positive Eu anomalies in seafloor sediment can be used as a tracer for hydrothermal influence due to divalent Eu partitioning into high-temperature hydrothermal fluid. Positive Eu anomalies relative to Post-Archean Australian Shale (PAAS) normalized REE concentrations are present in all sediment cores, which suggests that hydrothermal processes are influencing sediments > 200m from vent sites at Escanaba Trough. Even the samples with the lowest Eu/Eu* values are all greater than 0. Positive Eu anomalies were significantly greater in samples taken from cores recovered closest to hydrothermal mounds (mean=0.55) than those recovered farthest from hydrothermal mounds (mean=0.17) ($t(15)=3.4$, $p < .05$). However, the magnitude of the Eu anomalies differed based on dominant mineralogy of the subsample (Figure 28).

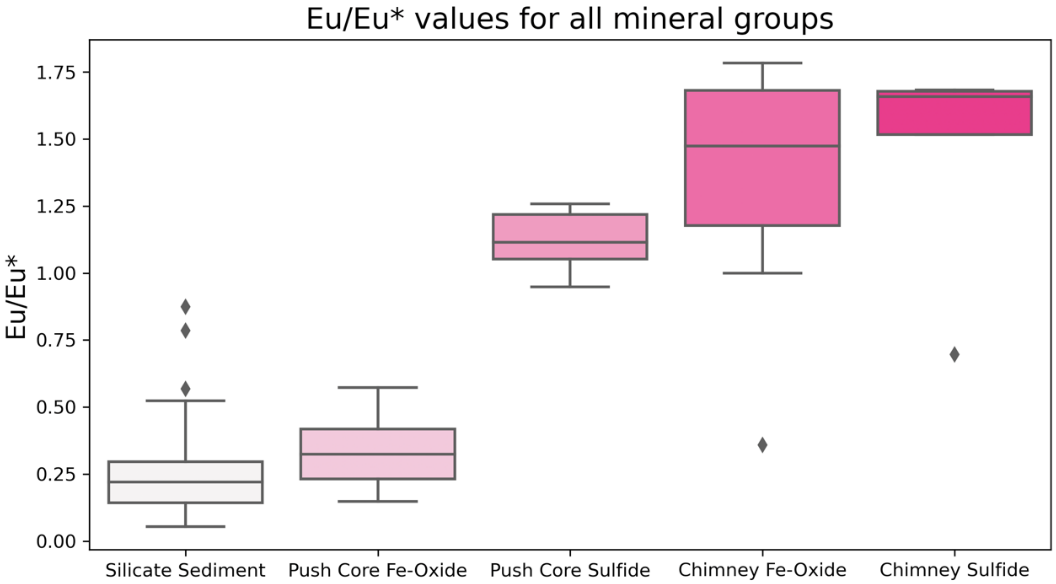

Figure 28. The boxes indicate the interquartile range of the Eu/Eu* values for mineral groups of interest, the horizontal line within each box shows the median value, and the whiskers extend to the furthest data points that are not considered outliers. Outliers are represented by diamond-shaped points.

This variation in Eu/Eu* values based on mineralogy was evident in dive 1418 (Figure 29). Eu/Eu* values were greatest in subsamples with sulfide mineralogy and smallest in samples with silicate sediment mineralogy. However, silicate sediment caps on cores J2-1418-PC03 and J2-1418-PC04 taken adjacent to the hydrothermal mound at Central Hill have Eu/Eu* values similar to those of sulfide samples.

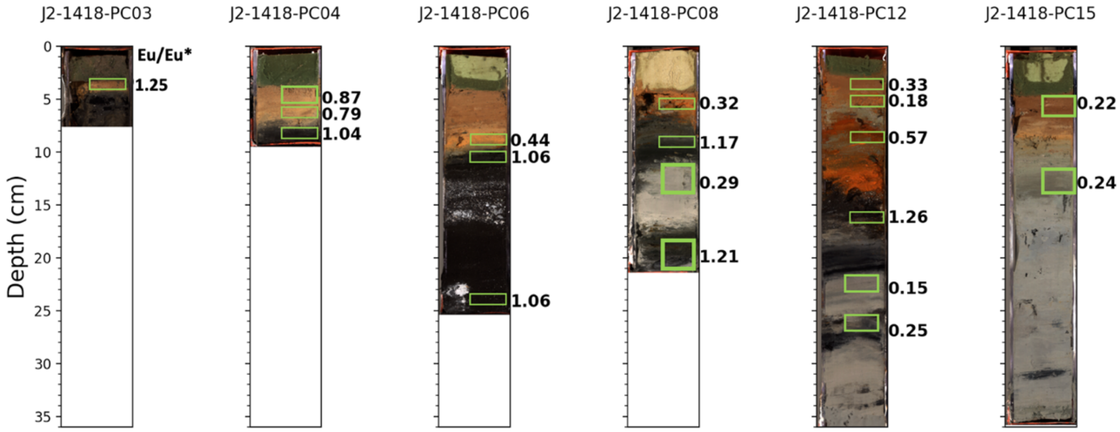

Figure 29. The Eu/Eu* value of each subsample from dive 1418 cores is shown to illustrate the variability of Eu anomalies within cores.

Sediment subsamples dominated by metal sulfides (XRD clusters 4 and 5) and Fe-oxides (XRD clusters 3 and 7) both exhibit positive Eu anomalies, although metal sulfide dominated samples have significantly greater Eu/Eu* values (mean=1.12) than Fe-oxide samples (mean=0.32) ($t(16) = 13.8$, $p < 0.05$) (Figure 28 and Figure 29). If Fe-oxide samples were formed from sulfide oxidation, the lower Eu/Eu* values could suggest that Eu is mobilized under oxidizing conditions. To further investigate this possibility, it is necessary to compare the mean Eu concentration of sediment sulfide and Fe-oxide samples. Sediment sulfide samples have significantly greater Eu concentrations (mean = 6.38 ppm) than sediment Fe-oxide samples (mean = 1.48 ppm) ($t(7) = 3.0$, $p < 0.05$) (Figure 30). Because the Eu/Eu* value is dependent on the abundance of Eu relative to Sm and Gd, we also report their respective concentrations. Sm concentrations are not significantly different between sulfide sediment (mean = 2.31 ppm) and Fe-oxide sediment (mean = 3.17 ppm) samples ($t(16) = 1.7$, $p > 0.05$). Similarly, Gd concentrations are not significantly different between sulfide sediment (mean = 2.1 ppm) and Fe-oxide sediment (mean = 3.1 ppm) samples ($t(16) = 2.0$, $p > 0.05$). When examining total REY concentrations in Fe-oxide (mean = 85.1 ppm) and sulfide sediments (73.2 ppm), no significant difference is observed ($t(16) = 0.8$, $p > 0.05$).

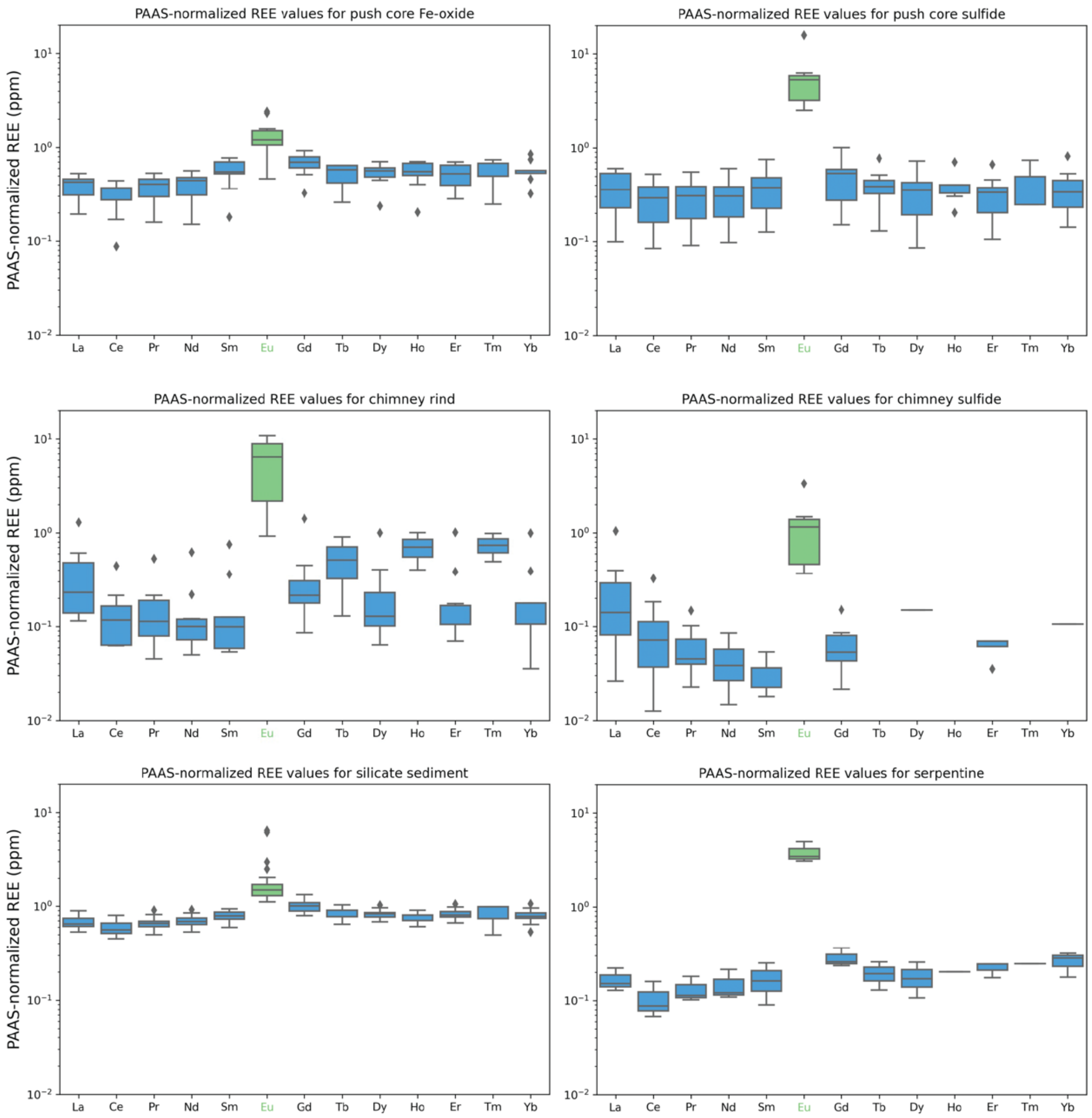

Figure 30. REE values for all sample types are shown. The Eu values are highlighted in green.

Although sediment subsamples have different mineralogies, all sediment subsamples include varying proportions of background sediments. To compare mineralogical variations in hydrothermal material with less background sediment influence, we also analyzed Eu anomalies and geochemical ratios for rocks collected from the hydrothermal chimneys and mounds. Of the 49 sulfide rock samples from Escanaba Trough, ten were subsampled for oxidized rind material on the exterior of the rock. Samples taken from the oxidized rinds of the sulfide rocks show opposing trends in total REY enrichment compared to metal sulfides and Fe-oxides products in push cores. The oxidized rinds of the sulfide rocks had significantly greater total REY concentrations (mean = 50.1 ppm) than bulk rock samples (mean = 18.4 ppm) ($t(15) = 2.4$, $p < 0.05$) (Figure 31). Si and Fe do not differ significantly between the rind and bulk samples of the sulfide rocks. Based on this finding, we suggest that oxide rinds that form during sulfide oxidation may scavenge REY elements from hydrothermal fluid. Alternatively, weathering may result in the loss of major elements and effectively concentrate REY elements in the remaining material.

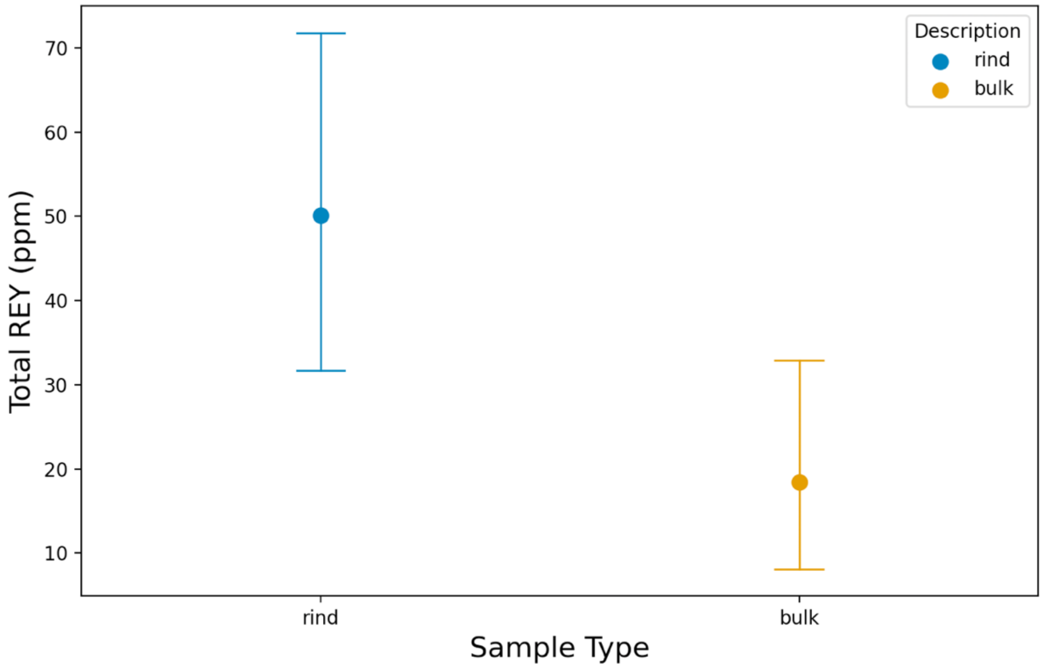

Figure 31. Mean and range of total REY in oxide rind and bulk sulfide rock samples from Escanaba Trough.

Some minor elements associated with sulfide minerals at Escanaba Trough are depleted in the oxide rind material, while others do not vary significantly in concentration. Cu is found in significantly lower concentrations in rinds (mean = 0.26 %) than in the bulk rock (mean = 1.45 %) ($t(13) = -2.6$, $p < 0.05$). Zn is also found in lower concentrations in rind samples (mean = 1.71 %) than in bulk rock samples (mean = 7.11 %) ($t(14) = -2.3$, $p < 0.05$). As and Pb concentrations do not differ significantly between rind and bulk samples.

5. Discussion

CT derived mass balance of hydrothermal material in push cores can show the surficial presence of hydrothermal material. A higher mass balance of hydrothermal material should be associated with proximity to the vent site that generated this material. The distance at which no hydrothermal material is evident should be considered as the maximum extent of the vent site's physical influence on the seabed. More intensive sampling could provide estimates of total sulfide mass at a given distance from the center of the vent site.

The influence of a hydrothermal vent system on the surrounding seabed varies between the different sites sampled at Escanaba Trough. Geochemical indicators in the form of Eu anomalies or the presence of hydrothermally derived minerals are used to indicate hydrothermal influence. Analyses of cores collected from abundant hydrothermal outcrops from Escanaba Trough indicate that accumulations of hydrothermal minerals that are discernable either visually or via CT scanning do not occur > 20 m from the edge of vent sites or have been buried under > 60 cm of sediment. The exception is near Central Hill, where hydrothermal material was recovered up to 60 m from the edge of the hydrothermal mound, but was not detected in a core 115 m from the edge of the mound. This was one of two sites where active venting was observed (Table 1). Similar work done by Gartman (In press) at Loki's Castle, a vent site in the Arctic Ocean, showed that the accumulation rate of hydrothermal material became indistinguishable from background sediment at > 200 m from the site of active venting.

If hydrothermally derived minerals and geochemical indicators are to be used as pathfinders for locating massive sulfides in inactive or extinct vent sites, it is important to understand how far they extend from vent sites. The evidence so far suggests that these characteristics are too confined to be useful in locating inactive or extinct vent sites on a regional scale. Ship or AUV-based geophysical methods likely offer a more effective way of locating these sites.

It is possible that other vent sites at Escanaba have hydrothermal mineralization greater than 20 m from the edge of the mound but are buried under > 60 cm of sediment (the maximum depth of push core recovery). Deeper drilling would be required to test this hypothesis. Cores from several drill holes were collected at Escanaba Trough during ODP Expedition 169 in 1996 (Zierenberg et al., 1998). Stringer zone mineralization and hydrothermal alteration of sediments were absent beneath massive sulfide at Escanaba Trough, although that expedition found sulfide mineralization as deep as 15 m below the seafloor in some locations (Zierenberg and Miller, 2000). It is unlikely that a scientific drillship will return to Escanaba Trough in the near future as, at the time of writing, the JOIDES Resolution is being retired with no plans for replacement. That said there are other drilling systems capable of recovering core at greater depths than push cores without need of a drill ship.

Another consideration in locating inactive or extinct vent sites is sulfide oxidation. If massive sulfides undergo extensive oxidation after precipitation on the seabed, their economically relevant metals will be mobilized in seawater. Sulfides minerals seen in Escanaba push cores showed varying states of oxidation. Sulfide chimneys directly exposed to seawater and buried sulfide in seawater appeared to undergo oxidation as evidenced by Fe-oxides adjacent to sulfide.

Oxidation via galvanic coupling has been experimentally observed in natural sulfide minerals (Gartman et al., 2020). This observation leads to a question of true stability versus rate of reaction. It’s uncertain which, if any, sulfides are stable under the conditions found at Escanaba Trough vent sites or if they are undergoing oxidation at varying rates. If the latter is the case, chimney rinds may be fully dissolved or fall away from the chimney once the oxidation of the less stable sulfides is complete. In this case, the rind provides a snapshot of the intermediate stage of oxidation. Alternatively, oxidation rinds could provide a protective mechanism against further oxidation by shielding interior sulfide minerals from oxidizing conditions. This uncertainty highlights the difficulty of interpreting the state of chemical reactions in samples analyzed. Determining the age of sulfide minerals at Escanaba trough would help with interpreting oxidation rates.

Hydrothermal mineral ages can be estimated using radium isotopes in barite (Jamieson et al., 2013). Age estimates can be used to determine timescales over which sulfides weather, both surficially at vents sites and buried under sediment. Constraining sulfide weathering rates under varying conditions can guide searches for prospective regions of sulfide preservation. Once age estimates are available, a more targeted coring campaign of distal vent site regions might help to locate regions of hydrothermal mineralization. Sedimentation rates at Escanaba Trough have been reported to fluctuate with sea level (Normark et al., 1994). Given our push core length of 60 cm, and an average sedimentation rate of 5 m/1000 yrs with higher rates >11 ka (Normark et al., 1994), the distal regions of inactive or extinct vent sites where venting ceased > 11 ka should be sufficiently sedimented to bury any hydrothermal material below the depth of push core recovery. The degree to which hydrothermal material is preserved will depend upon how reducing the subsurface environment is. Rapid sedimentation during the last sea-level low stand may have been sufficient to preserve accumulations of hydrothermally derived metal sulfides. Whether any preserved accumulations are of a large enough grade and size to constitute a deposit is an open question. Terrestrial analogs suggest they may exist in the modern ocean.

6. Conclusions

Escanaba Trough provides a unique opportunity to resolve the physical and chemical footprint of hydrothermal vent sites, due to the thick sediment accumulation and opportunity to sample direct hydrothermal precipitation and hydrothermal mass wasting processes surrounding areas of direct hydrothermal deposition. Large accumulations of hydrothermal massive sulfide are mostly restricted to the immediate vicinity of deposition, < 20 m from hydrothermal mounds. However, the geochemical signature of high-temperature vent fluid, indicated by europium anomalies in PAAS normalized rare earth element profiles, demonstrates that the entire Trough is influenced to some extent by high-temperature hydrothermal processes. Given the ubiquity of vent signatures in Escanaba Trough sediments and the limited extent of hydrothermal minerals beyond the edge of hydrothermal mounds, it is unlikely that these characteristics will be useful in locating inactive or extinct vent sites.

Bibliography

Allen, D. E., & Seyfried, W. E. (2005). REE controls in ultramafic hosted MOR hydrothermal systems: An experimental study at elevated temperature and pressure. Geochimica Et Cosmochimica Acta, 69(3), 675–683. https://doi.org/10.1016/j.gca.2004.07.016

American College of Radiology. (2023). GASTROINTESTINAL (GI) CONTRAST MEDIA IN ADULTS: INDICATIONS AND GUIDELINES. In *ACR Manual on Contrast Media* (pp. 62–81). Chapter. Retrieved October 11, 2023, from https://www.acr.org/-/media/ACR/Files/Clinical-Resources/Contrast_Media.pdf.

Bailey, E. B., & Grabham, G. W. (1909a). II.—Albitization of Basic Plagioclase Felspars. *Geological Magazine*, *6*(6), 250–256. https://doi.org/10.1017/s0016756800122551

Boas, F. E., & Fleischmann, D. (2012). CT artifacts: Causes and reduction techniques. *Imaging in Medicine*, *4*(2), 229–240. https://doi.org/10.2217/iim.12.13

Boström, K., Kraemer, T., & Gartner, S. (1973). Provenance and accumulation rates of opaline silica, Al, ti, Fe, Mn, Cu, ni and co in Pacific pelagic sediments. *Chemical Geology*, *11*(2), 123–148. https://doi.org/10.1016/0009-2541(73)90049-1

Clague, D. A., Zierenberg, R. A., Paduan, J. B., Caress, D. W., Cousens, B. L., Dreyer, B. M., Davis, A. S., McClain, J., & Ross, S. L. (2022). Emplacement and impacts of lava flows and intrusions on the sediment-buried Escanaba Segment of the Gorda mid-ocean ridge. *Journal of Volcanology and Geothermal Research*, *432*, 107701. https://doi.org/10.1016/j.jvolgeores.2022.107701

Corliss, J. B., Dymond, J., Gordon, L. I., Edmond, J. M., von Herzen, R. P., Ballard, R. D., ... & van Andel, T. H. (1979). Submarine thermal springs on the Galapagos Rift. *Science*, *203*(4385), 1073-1083.

Cox, D.P., & Singer, D.A. (1986). *Mineral Deposit Models*. United States Geological Survey.

Davis, E., & Villinger, H. (1992). Tectonic and Thermal Structure of the Middle Valley Sedimented Rift, Northern Juan de Fuca Ridge. In Proceedings of the Ocean Drilling Program. https://doi.org/10.2973/odp.proc.ir.139.102.1992

Davis, E., & Fisher, A. T. (1994). On the Nature and Consequences of Hydrothermal Circulation in the Middle Valley Sedimented Rift: Inferences from Geophysical and Geochemical Observations, Leg 139. In *Proceedings of the Ocean Drilling Program*. https://doi.org/10.2973/odp.proc.sr.139.259.1994

Deng, Y., Ren, J., Guo, Q., Cao, J., Wang, H., & Liu, C. (2017). Rare earth element geochemistry characteristics of seawater and porewater from deep sea in western Pacific. *Scientific Reports*, *7*(1). https://doi.org/10.1038/s41598-017-16379-1

Douville, É., Charlou, J., Oelkers, E. H., Bienvenu, P., Colón, C. F. J., Donval, J., Fouquet, Y., Prieur, D., & Appriou, P. (2002). The rainbow vent fluids (36°14′N, MAR): the influence of ultramafic rocks and phase separation on trace metal content in Mid-Atlantic Ridge hydrothermal fluids. Chemical Geology, 184(1–2), 37–48. https://doi.org/10.1016/s0009-2541(01)00351-5

Einsele, G., Gieskes, J. M., Curray, J. R., Moore, D., Aguayo, E., Aubry, M., Fornari, D. J., Guerrero, J., Kastner, M., Kelts, K., Lyle, M. W., Matoba, Y., Molina-Cruz, A., Niemitz, J. W., Rueda, J., Saunders, A. D., Schrader, H., Simoneit, B. R., & Vacquier, V. D. (1980). Intrusion of basaltic sills into highly porous sediments, and resulting hydrothermal activity. Nature, 283(5746), 441–445. https://doi.org/10.1038/283441a0

Findlay, A., Pellerin, A., Laufer, K., & Jørgensen, B. B. (2020). Quantification of sulphide oxidation rates in marine sediment. Geochimica Et Cosmochimica Acta, 280, 441–452. https://doi.org/10.1016/j.gca.2020.04.007

Fouquet, Y., Zierenberg, R.A., Miller, D.J., et al., 1998. Proc. ODP, Init. Repts., 169: College Station, TX (Ocean Drilling Program).

Gartman, A., Whisman, S. P., & Hein, J. R. (2020). Sphalerite Oxidation in Seawater with Covellite: Implications for Seafloor Massive Sulfide Deposits and Mine Waste. ACS Earth and Space Chemistry, 4(12), 2261–2269. https://doi.org/10.1021/acsearthspacechem.0c00177

German, C. R., Klinkhammer, G. P., Edmond, J. M., Mura, A., & Elderfield, H. (1990). Hydrothermal scavenging of rare-earth elements in the ocean. Nature, 345(6275), 516–518. https://doi.org/10.1038/345516a0

Goodfellow, W. D., & Zierenberg, R. A. (1997). Genesis of Massive Sulfide Deposits at Sediment-Covered Spreading Centers. In *Reviews in Economic Geology, Volcanic Associated Massive Sulfide Deposits: Processes and Examples in Modern and Ancient Settings* (Vol. 8). https://doi.org/10.5382/rev.08.13

Griffith, E., & Paytan, A. (2012). Barite in the ocean – occurrence, geochemistry and palaeoceanographic applications. *Sedimentology*, *59*(6), 1817–1835. https://doi.org/10.1111/j.1365-3091.2012.01327.x

Gurvich, E. G. (2006). *Metalliferous sediments of the world ocean: fundamental theory of deep-sea hydrothermal sedimentation*. Springer.

Hannington, M. D., De Ronde, C. D. J., & Petersen, S. (2005). Sea-Floor Tectonics and Submarine Hydrothermal Systems. In *Economic Geology 100th anniversary volume*. https://doi.org/10.5382/av100.06

Jamieson, J. W., & Gartman, A. (2020). Defining active, inactive, and extinct seafloor massive sulfide deposits. *Marine Policy*, *117*, 103926. https://doi.org/10.1016/j.marpol.2020.103926

Klinkhammer, G. P., Elderfield, H., Edmond, J. M., & Mitra, A. (1994). Geochemical implications of rare earth element patterns in hydrothermal fluids from mid-ocean ridges. *Geochimica Et Cosmochimica Acta*, *58*(23), 5105–5113. https://doi.org/10.1016/0016-7037(94)90297-6

Mosier, D. L., Berger, V. I., & Singer, D. A. (2009). Volcanogenic massive sulfide Deposits of the World – database and grade and tonnage models. *Open-file Report /*. https://doi.org/10.3133/ofr20091034

Karlin, R. E., Zierenberg, R. A., & Morton, J. L. (1994). *Sedimentation and neotectonism in the SESCA area, Escanaba Trough, southern Gorda Ridge* (Vol. 2022, pp. 131-142). US Department of the Interior.

Lonsdale, P., & Becker, K. (1985). Hydrothermal plumes, hot springs, and conductive heat flow in the Southern Trough of Guaymas Basin. Earth and Planetary Science Letters, 73(2–4), 211–225. https://doi.org/10.1016/0012-821x(85)90070-6

Monecke, T., Petersen, S., Hannington, M. D., Grant, H., & Samson, I. M. (2016). The Minor Element Endowment of Modern Sea-Floor Massive Sulfides and Comparison with Deposits Hosted in Ancient Volcanic Successions. *Rare Earth and Critical Elements in Ore Deposits*, *18*, 245–306. https://doi.org/10.5382/rev.18.11

Narendra, P. M., & Goldberg, M. (1977). A non-parametric clustering scheme for landsat. *Pattern Recognition*, *9*(4), 207–215. https://doi.org/10.1016/0031-3203(77)90005-x

Normark, W. R., Gutmacher, C. E., Zierenberg, R. A., Wong, F. L., Rosenbauer, R. J., & Morton, J. L. (1994). Sediment fill of Escanaba trough. *Geologic, Hydrothermal, and Biologic Studies at Escanaba Trough, Gorda Ridge, Offshore Northern California: US Geological Survey, Bulletin*, *2002*, 91-128.

Olivarez, A. M., & Owen, R. M. (1991). The Europium Anomaly of seawater: Implications for fluvial versus hydrothermal REE inputs to the oceans. *Chemical Geology*, *92*(4), 317–328. https://doi.org/10.1016/0009-2541(91)90076-4

Poppe, L. J., Paskevich, V., Hathaway, J. C., & Blackwood, D. (2001). A laboratory manual for X-ray powder diffraction. Open-file Report /. https://doi.org/10.3133/ofr0141

Taylor, S. R., & McLennan, S. M. (1995). The geochemical evolution of the continental crust. *Reviews of Geophysics*, *33*(2), 241–265. https://doi.org/10.1029/95rg00262

Tivey, M. (2007). Generation of seafloor hydrothermal vent fluids and associated mineral deposits. *Oceanography*, *20*(1), 50–65. https://doi.org/10.5670/oceanog.2007.80

Towell, D. G., Spirn, R. V., & Winchester, J. W. (1969b). Europium anomalies and the genesis of basalt: A discussion. *Chemical Geology*, *4*(3–4), 461–464. https://doi.org/10.1016/0009-2541(69)90012-6

Vallier, T., Harold, P., & Girdley, W. A. (1973). Provenances and dispersal patterns of turbidite sand in Escanaba Trough, northeastern Pacific Ocean. Marine Geology, 15(2), 67–87. https://doi.org/10.1016/0025-3227(73)90035-2

Van Dover, C. L. (2010). Mining seafloor massive sulphides and biodiversity: what is at risk? Ices Journal of Marine Science, 68(2), 341–348. https://doi.org/10.1093/icesjms/fsq086

Van Dover, C., Colaço, A., Collins, P. C., Croot, P., Meta×As, A., Murton, B. J., Swaddling, A., Boschen-Rose, R. E., Carlsson, J. E. L., Cuyvers, L., Fukushima, T., Gartman, A., Kennedy, R. M., Kriete, C., Mestre, N. C., Molodtsova, T. N., Myhrvold, A., Pelleter, E., Popoola, S., . . . Vermilye, J. (2020). Research is needed to inform environmental management of hydrothermally inactive and extinct polymetallic sulfide (PMS) deposits. Marine Policy, 121, 104183. https://doi.org/10.1016/j.marpol.2020.104183

Zierenberg, R. A., Koski, R. A., Morton, J. L., & Bouse, R. M. (1993). Genesis of massive sulfide deposits on a sediment-covered spreading center, Escanaba

Trough, southern Gorda Ridge. *Economic Geology and the Bulletin of the Society of Economic Geologists*, *88*(8), 2069–2098. https://doi.org/10.2113/gsecongeo.88.8.2069

Zierenberg, R. A., Fouquet, Y., Miller, D. J., Bahr, J. M., Baker, P. A., Bjerkgård, T., Brunner, C. A., Duckworth, R. C., Gable, R., Gieskes, J., Goodfellow, W. D., Gröschel-Becker, H. M., Guèrin, G., Ishibashi, J., Iturrino, G., James, R. H., Lackschewitz, K. S., Marquez, L. L., Nehlig, P., … Zuffa, G. G. (1998). The deep structure of a sea-floor hydrothermal deposit. *Nature*, *392*(6675), 485–488. https://doi.org/10.1038/33126

Zierenberg, R. A., & Reiss, C. A. (1994a). Geologic, hydrothermal, and biologic studies at Escanaba Trough, Gorda Ridge, offshore Northern California. *U.S. Geological Survey Bulletin 2022*. https://doi.org/10.3133/b2022

Zierenberg, R. A., Morton, J. L., Koski, R. A., & Ross, S. L. (1994b). Geologic setting of massive sulfide mineralization in the Escanaba Trough. *Geologic, hydrothermal, and biologic studies at Escanaba Trough, Gorda Ridge, offshore northern California*, 201-221.

Zierenberg, R.A., & Miller, D. J. (2000). Overview of Ocean Drilling Program leg 169: Sedimented Ridges II. *Proceedings of the Ocean Drilling Program, 169 Scientific Results*. https://doi.org/10.2973/odp.proc.sr.169.119.20

Tables

Table 1 Dive numbers with associated names and locations.

Dive	**Location**	**Classification**
1418 (Central Hill)	41.00013, -127.49468	Active
1419 (Edifice Rex)	41.06394, -127.49910	Inactive
1420 (Edifice Rex)	41.07998, -127.45159	Inactive
1421 (SESCA Hill S3A)	40.69872, -127.52798	Active
1422 (SESCA Hill S2A)	40.77436, -127.53559	Inactive
1424 (SESCA Unnamed/North Hill)	40.79030, -127.50515	Inactive
1425 (Central Hill)	40.99161, -127.49348	Inactive
1426 (MESCA)	40.88927, -127.51760	Inactive

Table 2 Work completed by the author.

Shipboard	Sat ROV watches, electrochemical profiling of sediment cores.
CT Scanning	Loaded cores in CT scanner, processed, plotted, and analyzed CT data.
XRD	Packed and loaded crushed samples in XRD.
Mineralogical Analyses	Clay mineralogy identification and microscopy.
Geochemical Analyses	Calculated Eu anomalies, geochemical ratios, and statistics presented here

Table 3 The dominant mineralogy of each cluster of sediment subsamples, obtained from powder X-ray diffraction.

XRD Cluster	**Dominant Mineralogy**
Cluster 1	Quartz, albite, chlorite-serpentine, muscovite, illite
Cluster 2	Quartz, albite, chlorite-serpentine, muscovite, ferrihydrite
Cluster 3	Ferrihydrite, Quartz, chlorite-serpentine, albite, muscovite
Cluster 4	Pyrrhotite, quartz, barite, isocubanite, magnetite, clinochlore, illite, albite
Cluster 5	Pyrrhotite, barite, isocubanite, clinochlore, albite, magnetite, quartz
Cluster 6	Clino-chrysotile, talc/sepiolite, chlorite-serpentine
Cluster 7	Goethite, unknown clay, talc/sepiolite, ferrihydrite

Table 4 The weight percent of Fe, Si, and S are shown for sediment subsamples in the Fe-oxide, metal sulfide, and silicate XRD clusters.

Major Elements in Sediments (mean)	**Fe**	**Si**	**S**
Fe-Oxide (n = 10)	21.5 %	15.84 %	0.46 %

Metal Sulfide (n = 8)	30.04 %	9.25 %	16.48 %
Silicate (n = 31)	5.56 %	25.51 %	0.84 %

Table 5 The weight percent of Fe, Si, and S are shown for the bulk and rind components of rock samples from Escanaba Trough.

Major Elements in Bulk and Rind (mean)	**Fe**	**Si**	**S**
Bulk (n = 10)	27.69 %	2.05 %	26.62 %
Rind (n = 10)	22.17 %	2.56 %	4.74 %

Table 6 The weight percent of As, Cu, and Zn are shown for the bulk and rind components of rock samples from Escanaba Trough.

Minor Elements in Bulk and Rind (mean)	**As**	**Cu**	**Zn**
Bulk (n = 10)	1.86 %	1.45 %	7.11 %
Rind (n = 10)	2.33 %	0.26 %	1.71 %